
Computer Science

**Carnegie
Mellon**

DTIC QUALITY INSPECTED 2

DISTRIBUTION STATEMENT A
Approved for Public Release
Distribution Unlimited

A Numerical Optimization Approach to General Graph Drawing

Daniel Tunkelang

January 1999

CMU-CS-98-189

School of Computer Science

Carnegie Mellon University

Pittsburgh, PA 15213

*Submitted in partial fulfillment of the requirements
for the degree of Doctor of Philosophy*

Thesis Committee:

Daniel Sleator, Chair

Paul Heckbert

Bruce Maggs

Omar Ghattas, Civil and Environmental Engineering

Mark Wegman, IBM T. J. Watson Research Center

Copyright © 1999 Daniel Tunkelang

This research was supported by the National Science Foundation under grant number DMS-9509581. The views and conclusions contained in this document are those of the author and should not be interpreted as representing the official policies, either expressed or implied, of the NAF or the U.S. government.

DISTRIBUTION STATEMENT A
Approved for Public Release
Distribution Unlimited

19990802 075

Keywords: visualization, graph drawing, numerical optimization, force-directed



School of Computer Science

DOCTORAL THESIS
in the field of
ALGORITHMS, COMBINATORICS AND OPTIMIZATION

*A Numerical Optimization Approach to
General Graph Drawing*

DANIEL TUNKELANG

Submitted in Partial Fulfillment of the Requirements
for the Degree of Doctor of Philosophy

ACCEPTED:

Daniel Sleator
THESIS COMMITTEE CHAIR

Nov, 19, 1998
DATE

M. Hene
DEPARTMENT HEAD

1/12/99
DATE

APPROVED:

R. Rly
DEAN

1/8/99
DATE

Abstract

Graphs are ubiquitous, finding applications in domains ranging from software engineering to computational biology. While graph theory and graph algorithms are some of the oldest, most studied fields in computer science, the problem of visualizing graphs is comparatively young. This problem, known as *graph drawing*, is that of transforming combinatorial graphs into geometric drawings for the purpose of visualization.

Most published algorithms for drawing general graphs model the drawing problem with a physical analogy, representing a graph as a system of springs and other physical elements and then simulating the relaxation of this physical system. Solving the graph drawing problem involves both choosing a physical model and then using numerical optimization to simulate the physical system.

In this dissertation, we improve on existing algorithms for drawing general graphs. The improvements fall into three categories: speed, drawing quality, and flexibility. We improve the speed using known techniques from both the many-body work in astrophysics and the numerical optimization literature. We improve drawing quality both by making our physical model more comprehensive than those in the literature and by employing heuristics in our optimization procedure to avoid poor local minima. Finally, we improve the flexibility of existing approaches both by cleanly separating the physical model from the optimization procedure and by allowing the model to include a broad class of constraints.

We are able to demonstrate some of our improvements through theoretical analysis. To demonstrate the others, we use an implementation of our approach in the Java programming language.

Acknowledgments

First, I would like to thank my advisor, Danny Sleator, and the other members of my committee: Paul Heckbert, Omar Ghattas, Bruce Maggs, and Mark Wegman. I am especially grateful that they allowed me to pursue a dissertation in an area somewhat removed from their primary fields of research, advising me according to their respective strengths. Their feedback was essential to the quality of this dissertation.

I am greatly indebted to Carnegie Mellon University for providing both the funding and the intellectual environment that were essential to my work. I especially thank my former housemate, Jonathan Shewchuk, and my officemates, Girija Narlikar and Chris Okasaki, for engaging me in discussions across the gamut of computer science. A list of all of the people who formed my experience at CMU would double this size of this dissertation, but some names are indispensable: Avrim Blum, Andrew Kompanek, Corey Kosak, Sean Slattery, and Alma Whitten.

I owe my interest in graph drawing to Mark Wegman, who introduced me to the area when I was an MIT undergraduate co-op student at the IBM T. J. Watson Research Center. I thank Mark and Charles Leiserson again for supervising my Master's Thesis, and I thank others at IBM for numerous discussions and encouragement: Rangachari Anand, Lisa Brown, Roy Byrd, Jim Cooper, Doug Kimmelman, Alan Marwick, V. T. Rajan, and Tova Roth.

My family and friends have always been invaluable, but especially during the ordeal of completing my dissertation. I cannot thank my parents and brother enough for putting up with my ever-changing moods during this trying time. Likewise, my closest friends, Marissa Billowitz and Bilal Khan, sustained me through many trying days and nights.

Finally, I would like to thank all of the teachers who nurtured my interests in mathematics and computer science through two decades of schooling. Above all, I thank Gian-Carlo Rota, whom I can finally take up on his promise to let me take him out to dinner after obtaining my Ph.D.

Table of Contents

1. Introduction.....	7
2. What is Graph Drawing?	9
2.1. Drawing Conventions.....	12
2.2. Constraints.....	13
2.3. Preferences	14
2.4. Summary.....	15
3. Previous Work.....	16
3.1. Algorithms for Specific Classes of Graphs	16
3.1.1. Trees	16
3.1.2. Directed Acyclic Graphs.....	18
3.1.3. Planar Graphs.....	20
3.2. Algorithms for General Graphs.....	21
3.2.1. The Topology-Shapes-Metrics Approach.....	21
3.2.2. The Force-Directed Approach	22
4. The Force-Directed Approach	23
4.1. The Spring Embedder Model	23
4.2. Kamada and Kawai's Approach.....	24
4.3. Fruchterman and Reingold's Approach	25
4.4. Models that Address Edge Crossings.....	26
4.5. Computational Complexity	26
4.6. Other Force-Directed Work.....	27
4.7. Summary of Problems in Published Approaches	27
5. Modeling Graph Drawing as an Optimization Problem	29
5.1. Output Variables	29
5.2. Force Laws	29
5.2.1. Springs	30
5.2.2. Vertex-Vertex Repulsion	32
5.2.3. Vertex-Edge Repulsion.....	34
5.3. Constraints.....	35
5.3.1. Penalty Functions.....	35
5.3.2. Constraints versus Preferences	35
6. Computing the Gradient Efficiently.....	37
6.1. Computing the Gradient Naïvely.....	37
6.2. Simple $\theta(n)$ Approximations for Computing Vertex-Vertex Repulsion.....	38
6.2.1. Distance Cut-Offs	38
6.2.2. Centripetal Repulsion	40

6.3. Approximating Vertex-Vertex Repulsion Forces in $\theta(n \log n)$ Time	42
6.3.1. Building the Quad-Tree	43
6.3.2. Computing the Force on Each Particle	45
6.3.3. Applying Barnes-Hut to Compute Vertex-Vertex Repulsion Forces	47
6.4. Computing Vertex-Edge Repulsion Forces	47
7. The Optimization Procedure	49
7.1. The Method of Steepest Descent	49
7.2. The Newton Direction	51
7.3. The Conjugate Gradient Method	52
7.4. The Conjugate Gradient Method with Restarts	53
7.5. Computing the Step Size	54
8. Making the Gradient Time-Dependent	56
8.1. Making the Gradient Smoother in the Early Iterations	56
8.1.1. Capping Spikes	57
8.1.2. Strengthening the Long-Range Vertex-Vertex Repulsion Forces	58
8.2. Using Exterior Penalties to Incorporate Constraints	58
8.3. Introducing Additional Degrees of Freedom	60
9. Vertex Size and Shape	62
9.1. Vertex Radii	62
9.2. Adapting the Force Laws to Consider Vertex Radii	63
9.2.1. Increasing the Rest Length of Edge Springs	63
9.2.2. Modifying the Vertex-Vertex Repulsion Law	64
9.2.3. Modifying the Vertex-Vertex Repulsion Law	64
9.3. Adapting the Procedure to Compute the Forces	65
10. Qualitative Results: A Gallery of Examples	66
10.1. Trees	66
10.2. Planar Biconnected Graphs	69
10.3. Sparse Non-Planar Graphs	72
10.4. Dense Graphs	74
11. Quantitative Results	77
11.1. Computational Complexity	77
11.2. Number of Iterations	78
11.3. Running Time	82
12. Conclusions and Future Work	84
Bibliography	87

1. Introduction

In 1979, Wetherell and Shannon concluded a paper on “Tidy Drawing of Trees” by saying, “We are currently studying methods for the tidy display of other graph structures, a subject not covered in the literature” [WS79]. In the past two decades, graph drawing has become a vibrant research area. An annotated bibliography from 1994 [DETT94] lists over 300 relevant publications, and these do not include the dozens of papers and systems presented at the annual symposia on graph drawing since 1993. More recently, the authors of the bibliography have published a textbook [DETT99] on graph drawing.

Most of the work, however, considers special cases. A quarter of the papers in the annotated bibliography address the problem of computing planar (crossing-free) drawings of planar graphs. A comparable fraction of the work considers layered drawings of directed acyclic graphs. While this specificity attests to the relative importance of certain classes of graphs, it also reflects the difficulty of solving the general problem.

Our work addresses general graph drawing. Although the treatment of special cases can lead to elegant mathematical results, the practical side of graph drawing requires a greater emphasis on generality. Our approach, based on numerical optimization, builds on existing approaches for drawing general graphs. We demonstrate the value of our work in three ways. First, we show both a theoretical and an empirical improvement in performance over the published general graph drawing algorithms. Second, we achieve better drawings by incorporating aesthetic elements that the published approaches do not take into account. Third, we obtain a more flexible approach by using a numerical optimization approach that cleanly separates the objective function from the optimization procedure and allows us to incorporate a general class of constraints into our model.

We begin with an overview of the graph drawing problem and its wide range of applications. We then review the previous work in the field, focusing on algorithms that address general graphs. We present a general framework for modeling graph drawing as a numerical optimization problem, and we show how previous approaches fit into this framework. We then present our techniques to address performance, drawing quality, and flexibility. Our principle solutions for the performance problem are to use the Barnes-Hut procedure to reduce a $\theta(n^2)$ time computation in the inner loop to $\theta(n \log n)$, and then to replace the commonly used method of steepest descent with the conjugate gradient method as a more efficient optimization procedure. Our main improvements in

drawing quality come from incorporating vertex-edge distance and vertex shape into our physical model. Finally, we describe how we incorporate a general class of constraints into our model by making the objective function time-dependent and using the method of exterior penalties. In fact, this technique of using a time-dependent objective function not only makes our approach more flexible, but can also improve both performance and drawing quality. We present the results of our work both qualitatively, through a gallery of examples, and quantitatively, through both theoretical and empirical analysis.

2. What is Graph Drawing?

Before we can talk about graph drawing, we must explain what we mean by a graph. A *graph* is a collection of entities and their relationships. We refer to the entities as the *vertices* of the graph, and to their relationships as *edges*.¹ Each edge pairs two vertices, which we call its *endpoints*. When we are discussing a single graph, we will denote it by G , and we will denote the vertex and edge sets as V and E respectively.

In the simplest case, the vertices and edges have no further information associated with them. For example, we can describe the complete bipartite graph $K_{3,3}$ by enumerating its vertices $V = \{1, 2, 3, 4, 5, 6\}$ and edges $E = \{(1, 4), (1, 5), (1, 6), (2, 4), (2, 5), (2, 6), (3, 4), (3, 5), (3, 6)\}$. Here, the vertex names are just placeholders, since the vertices are indistinguishable except where the topology of the graph breaks their symmetry. Figure 2.1 shows a drawing of $K_{3,3}$.

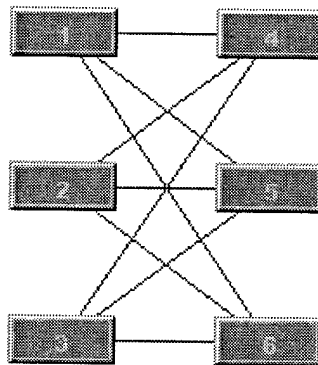


Figure 2.1: A Drawing of $K_{3,3}$

In a more typical context, the vertices and edges will have further information associated with them—often information that is essential to the sense of the graph. For example, we could have a graph where the vertices represent web pages and the edges are links connecting them. Here, each vertex would be associated with a URL and possibly further attributes, such as the type of its associated document. Another possibility is that the

¹ Other authors refer to vertices as *nodes* and to edges as *arcs* or *links*. Our terminology is consistent with using the letters V and E to denote the vertex and edge sets, as well as the lowercase letters v and e for individual vertices and edges.

graph could represent a database of terms extracted from a large corpus of text. Here, the edges could store the nature of the relationships among the terms. Figures 2.2 and 2.3 show examples of graphs that could arise in practical applications.

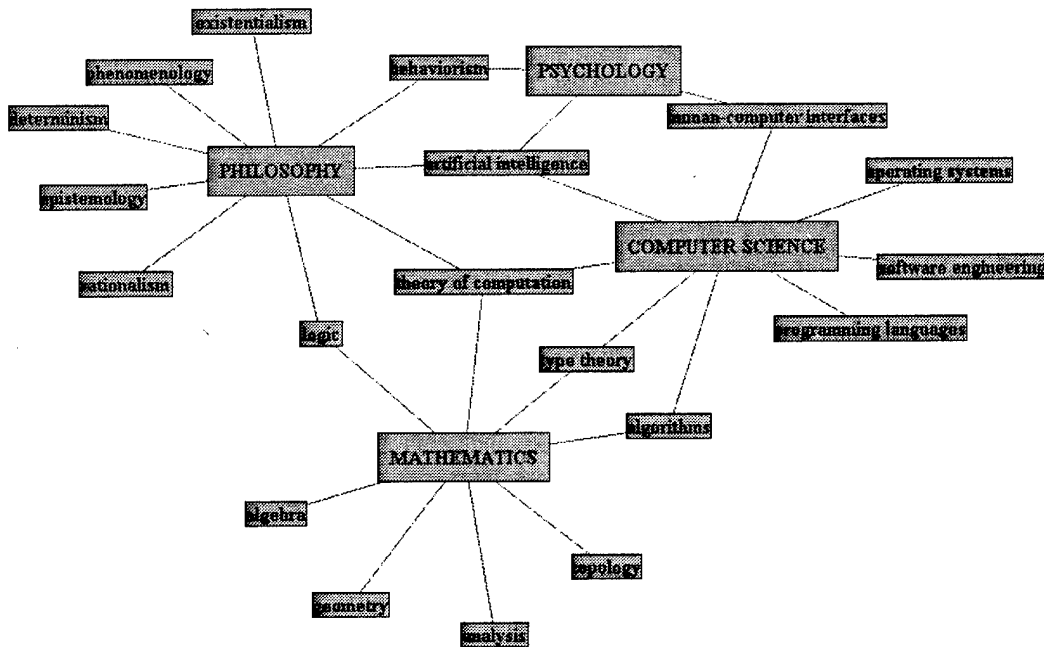


Figure 2.2: Disciplines and their Common Subfields

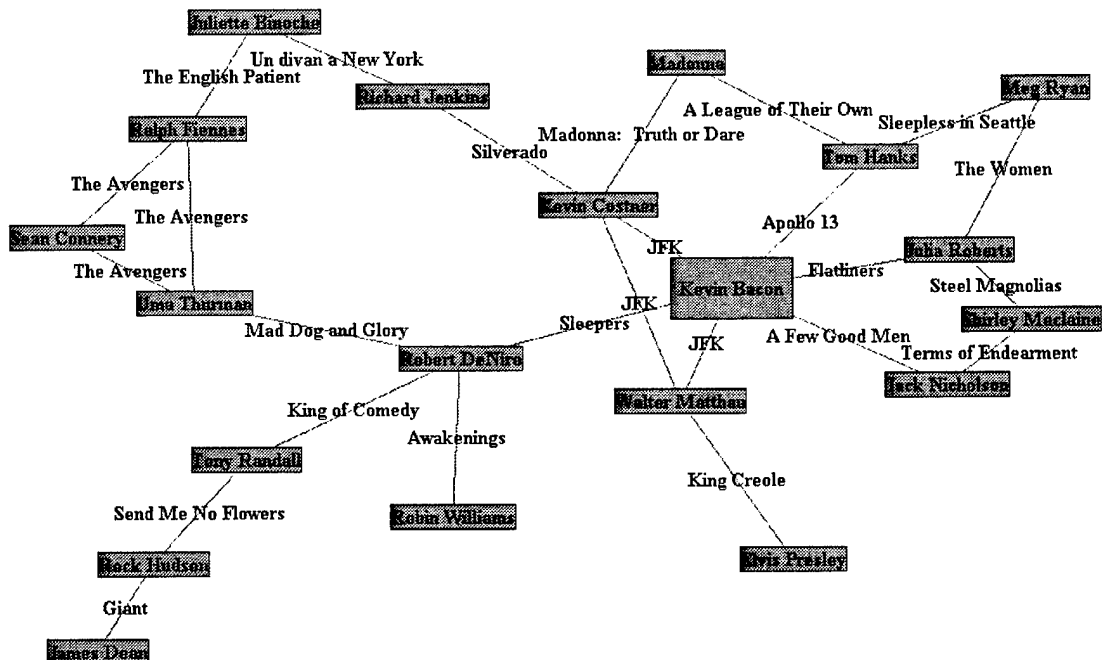


Figure 2.3: Six Degrees of Kevin Bacon

One attribute of an edge that we single out is its directedness. An edge can be *undirected* or *directed*, reflecting whether the relationship between the endpoints is symmetric or asymmetric. We call a graph consisting of only undirected edges an *undirected graph* and one consisting of only directed edges a *directed graph*. If a graph has both undirected and directed edges, we call it a *mixed graph*. In this dissertation, we will focus on undirected graphs. The techniques we describe can be used to draw directed graphs as well, but other work, which we describe in the following chapter, is more suited to drawing directed graphs in such a way as to emphasize the directions of edges.

We define *graph drawing* as the transformation of a graph into a visual representation of the graph, which we call a *drawing*. We depict this transformation in Figure 2.4. In a typical drawing, we map vertices to boxes or circles on a subset of the plane and map edges to lines connecting the boxes that represent their endpoints.

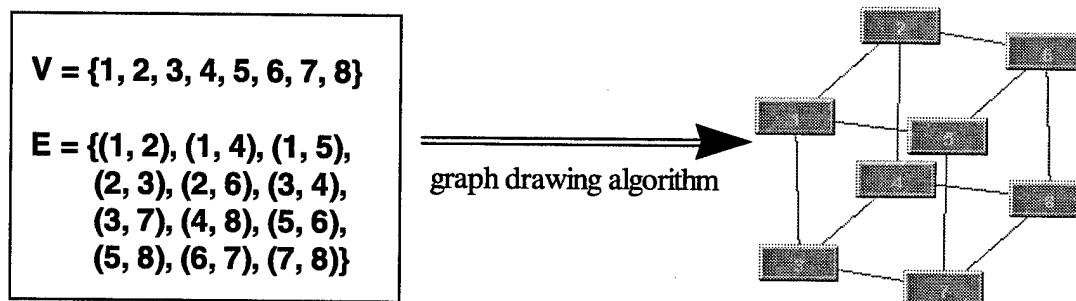


Figure 2.4: Graph Drawing

Although graph drawing per se is a young field of research, graph drawing as a practical art predates computer science. Throughout the sciences, people use graphs to represent systems composed of a large number of interacting components, especially when the individual components are simple. Physicists and chemists draw graphs that model interaction among particles. Electrical engineers draw graphs to represent circuits. Social scientists draw graphs of group interaction. Still, the widest use of graph drawing is in computer science and information technology, with domains ranging from software architecture to semantic networks. Often, graphical visualizations of such systems reveal far more structure than textual ones, as per the cliché that a picture is worth a thousand words.

Di Battista et al. break down graph drawing requirements into three basic concepts: drawing conventions, aesthetics, and constraints [DETT99]. We briefly describe each of these concepts.

2.1. Drawing Conventions

Drawing conventions are the basic rules that define the space of admissible drawings. Generally, we can think of drawing conventions as global constraints on the space of drawings. The drawing conventions specify, among other things, the area that can be used for the drawing. Unless we specify otherwise, we will assume that the drawing area is a rectangle in the Euclidean plane \mathbf{R}^2 .

Di Battista et al. list some of the more widely used drawing conventions, and Figure 2.5 shows various drawings of the complete graph K_4 , for which $V = \{1, 2, 3, 4\}$ and $E = \{(1, 2), (1, 3), (1, 4), (2, 3), (2, 4), (3, 4)\}$, using some of these conventions:

Polyline Drawing: each edge is represented as a chain of connected line segments; the chain may bend at the connection points. See Figure 2.5 (a).

Straight-line Drawing: each edge is represented as a single line segment. A special case of polyline drawing. See Figure 2.5 (b).

Orthogonal Drawing: each edge is represented as chain of alternating horizontal and vertical line segments. A special case of polyline drawing. See Figure 2.5 (c).

Planar drawing: no two edges cross; requires that the graph be planar. See Figure 2.5 (d).

Upward drawing: all directed edges are represented by lines or curves that strictly increase in the vertical direction. Requires that the graph have no directed cycles. See Figure 2.5 (e) below.

Grid Drawing: all vertices, edge crossings, and bend-points have integer coordinates.

Generally, our drawing conventions will include some subset of the above, as well as other application-dependent considerations. Our main interest will be in straight-line and upward drawings, since these conventions are the most amenable to numerical optimization approaches.

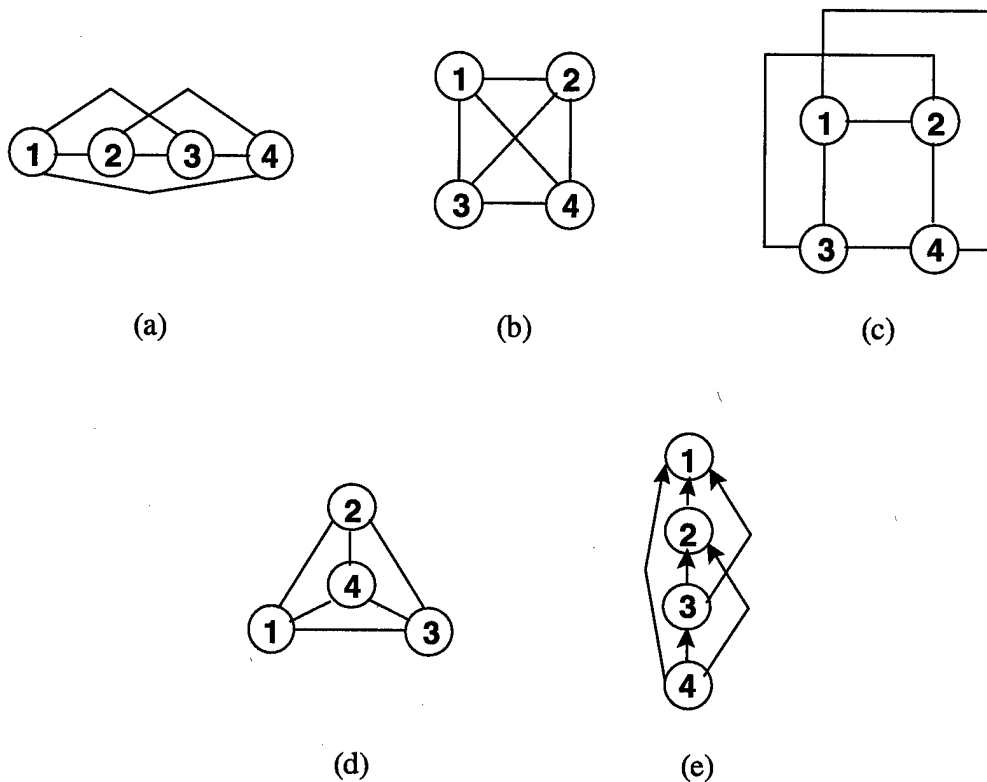


Figure 2.5: Illustration of Various Drawing Conventions for the Graph K_4

We note that none of the above conventions address vertex shape. We will assume that vertices are represented by circles, ellipses, or rectangles. Often, we will use the space taken up by a vertex to show a name or some other information (textual or pictorial) associated with it.

2.2. Constraints

The drawing conventions constrain the general properties of the drawing. Sometimes, we use explicit *constraints* to specify the behavior of particular vertices, edges, or subgraphs.

The two primary sources of constraints are semantics and user interaction. Semantics, for example, might dictate that a given subset of vertices forms a cluster and should be drawn in a rectangle that does not include any other vertices. A user, after seeing an automatically produced drawing might decide that the drawing looks better if a particular vertex is placed to the left of another vertex and then request that the drawing be recomputed subject to that constraint. Typical constraints concern absolute or relative vertex placement.

2.3. Preferences

While it is possible for drawing conventions and constraints to fully determine a drawing, it is often more useful to distinguish between hard constraints and soft preferences. For example, we could impose a constraint specifying the exact distance between two vertices in the drawing, or we could incorporate a preference that the distance between the vertices be close to the desired distance. Preferences have two advantages over constraints. First, they can be associated with continuous functions, as in the previous example, while constraint satisfaction is binary. Second, they can always be combined, even when combining analogous constraints might lead to an inconsistency. For example, minimizing edge lengths and maximizing the distances between all vertices are clearly competing goals; they can, however, be combined in the form of weighted preferences.

Generally speaking, a *preference* specifies a measure by which we can judge a drawing. We quantify these preferences by making them weighted terms in an *objective function* that measures the overall quality of a drawing. The weights reflect the priority assigned to each preference.

Di Battista et al. list the following widely used preferences, which they call “aesthetics”:

Crossings: minimization of the number of edge crossings.

Area: minimization of the drawing area. Measured using either the convex hull or the bounding rectangle. Only meaningful when the drawing conventions prevent the drawing from being arbitrarily scaled down.

Total Edge Length: minimization of the sums of lengths of edges. Only meaningful when the drawing conventions prevent the drawing from being arbitrarily scaled down.

Maximum Edge Length: minimization of the maximum lengths of an edge. Only meaningful when the drawing conventions prevent the drawing from being arbitrarily scaled down.

Uniform Edge Length: minimization of the variance in edge length. Only meaningful when the drawing conventions prevent the drawing from being arbitrarily scaled down.

Total Bends: minimization of the total number of edge bends in a polyline drawing.

Maximum Bends: minimization of the maximum number of edge bends per edge in a polyline drawing.

Uniform Bends: minimization of the variance in the number of edge bends in a polyline drawing.

Angular Resolution: maximization of the minimum angle between edges incident to the same vertex in a polyline (especially straight-line) drawing.

Aspect Ratio: minimization of the ratio between the larger and smaller dimensions of the drawing area.

Symmetry: displaying symmetries of the graph with geometric symmetries.

The sheer variety of criteria enumerated above suggests that aesthetics are more of an art than a science. Given the subjective nature of aesthetics, there are limits to how systematic an approach we can take to describing what makes one drawing of a graph better than another. Nonetheless, these criteria are sufficiently general that we can start from some subset of them, refining our model to suit the needs of a particular application.

2.4. Summary

By quantifying and combining drawing conventions, constraints, and preferences, we arrive at formulation of graph drawing as a problem in numerical optimization. The drawing conventions dictate the variables in our problem space. The constraints define the feasible portion of the problem space. Finally, the objective function expresses the weighted combination of preferences and defines the overall measure that we seek to minimize, subject to the constraints.

3. Previous Work

Although graph drawing as such is a young field, it has already generated a substantial body of literature. The best general sources of information are the annotated bibliography [DETT94], the recently published textbook [DETT99], and the proceedings of the annual Symposia on Graph Drawing [GD93, GD94, GD95, GD96, GD97, GD98]. Related fields include computational geometry, combinatorial optimization, visual languages, and human-computer interfaces. This section describes the small fraction of that work that is most relevant to the proposed approaches; the reader is encouraged to consult the above references.

Broadly speaking, there are two kinds of graph drawing algorithms. The first address specific classes of graphs. Algorithms of the second kind address general graphs and differ mostly in their choice of optimization strategy.

All of the algorithms that we discuss produce drawings in \mathbf{R}^2 , with vertices represented as non-overlapping circles (or boxes) and edges as open curves connecting them. They generally assume that the input graphs are connected, since it is not difficult to compute the connected components of a graph and draw them separately.

3.1. Algorithms for Specific Classes of Graphs

There are a variety of algorithms designed for specific classes of input graphs. Three classes that have attracted particular attention are trees, directed acyclic graphs, and planar graphs.

3.1.1. Trees

Trees, the simplest class of connected graphs, are among the most common structures in computer science. A *tree* is a connected, acyclic graph. Most algorithms for drawing trees assume that all edges are drawn as straight lines directed away from a specified root vertex. Supowit and Reingold [SR83] outline six widely accepted aesthetic constraints for what they call a “eumorphous” (well-shaped) drawing of a rooted tree:

- 1) The height of a vertex (i.e. its vertical distance from the root) should be proportional to its distance from the root measured in tree branches. Hence, vertices are placed on discrete horizontal levels.

- 2) When the children are ordered (e.g. in a binary tree), left children should be placed strictly to the left of their parents. Similarly, right children should be placed strictly to the right.
- 3) Vertices on a level should have some minimum separation so as not to overlap.
- 4) Parents should be centered over their children.
- 5) Edges should not cross, i.e. the drawing should respect the planarity of the tree.
- 6) Isomorphic subtrees should be drawn congruently, and subtrees that are isomorphic when the order of children in all of their subtrees is reversed should be drawn as mirror images.

Figure 3.1 illustrates a eumorphous drawing of a rooted tree.

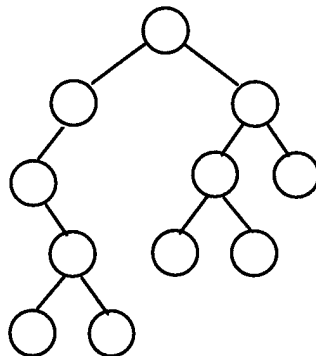


Figure 3.1: Eumorphous Drawing of Rooted Tree

Supowit and Reingold, along with other researchers, aim to minimize the width of the tree subject to these constraints. The linear-time algorithm of Reingold and Tilford [RT81] satisfies the six constraints but does not achieve the optimal width. Supowit and Reingold show that, if vertex positions can be arbitrary real numbers, then the width minimization problem can be solved in polynomial time by linear programming [SR83]. They show that, if the vertex positions are restricted to the integer lattice, then the problem is NP-complete.

The problem of drawing free trees—that is, trees without a specified root—has received far less attention. Eades describes an approach for drawing free trees radially in [Ea92]. The algorithm first picks as a root the graph-theoretical center of the tree—that is, a vertex that minimizes the height of the tree directed outwards from that vertex. If there is more than one center, then the algorithm chooses among them arbitrarily. It then places the remaining vertices on concentric circles around the chosen root. Edges are drawn as straight lines. The algorithm respects the tree’s planarity as a constraint and seeks to minimize the variation in edge length. The algorithm draws the tree recursively in linear time. Figure 3.2 illustrates a radial drawing of a free tree.

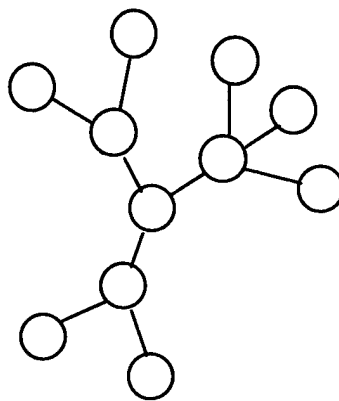


Figure 3.2: Radial Drawing of a Free Tree

3.1.2. Directed Acyclic Graphs

Directed acyclic graphs, like rooted trees, have an inherent direction of flow. They are generally used to represent hierarchical structures. Their drawing conventions are similar to those for rooted trees, only that, since the graph may not be planar, the constraint of planarity is replaced with a preference for avoiding edge crossings.

The standard approach, originally proposed by Sugiyama et al. [STT81], consists of three phases that are illustrated in Figure 3.3.

The first phase assigns the vertices to levels such that every edge is directed “upwards”—that is, from a lower level to a higher one. This phase also creates “dummy vertices” as necessary along the edges so that all edges connect vertices (real or dummy) on consecutive layers. A long edge (v_i, v_j) is thus transformed into a chain of short edges (v_i, dummy_1) , $(\text{dummy}_1, \text{dummy}_2)$, ..., (dummy_k, v_j) , where k is the number of intermediate levels separating the two vertices. Sugiyama’s original approach uses a

longest-path layering—that is, the level of a vertex corresponds to the number of edges in the longest directed path entering the vertex. Gansner et al. propose, as an alternative layering method, using linear programming to minimize the total number of dummy vertices [GNV88].

The second phase determines the ordering of the vertices on each horizontal layer with the goal of minimizing the number of edge crossings. Two heuristics for this problem, which is NP-complete [GJ83], are to iteratively sort vertices according to the mean or median positions of their neighbors on adjacent levels.

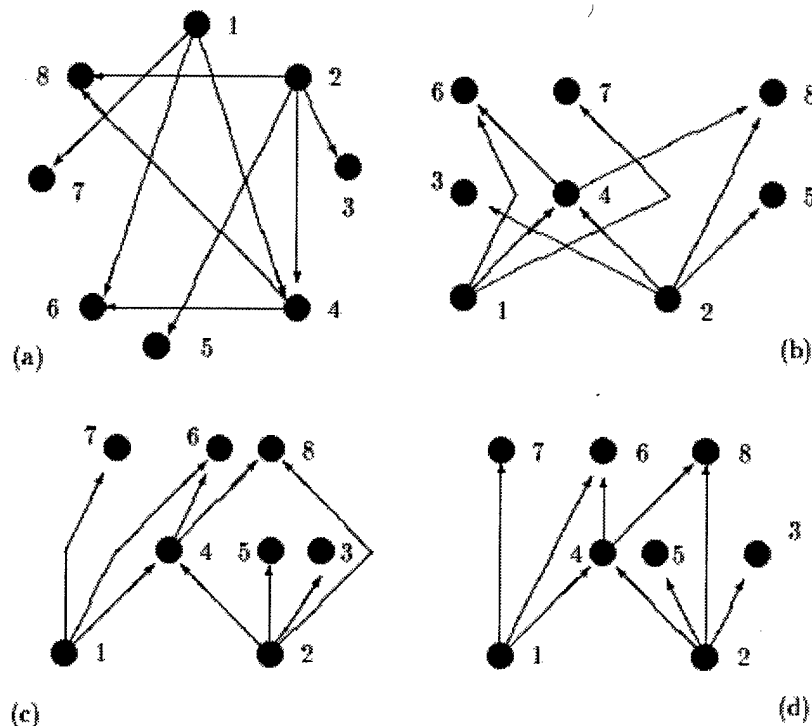


Figure 3.3: Drawing a Directed Acyclic Graph [DETT94]

(a) original drawing (b) arrangement of vertices in layers
(c) vertices permuted to avoid crossings (d) final drawing

The third phase uses the layering and ordering constraints of the previous two phases to compute a drawing. The usual goal is to minimize the horizontal lengths of edges and the number of bends induced by dummy vertices. Many heuristics have been proposed for this last step, ranging from linear programming to physically-based simulation. Finally, the edges are drawn either as straight lines, polylines that bend at the dummy vertices, or splines interpolated from the polylines.

The first and third phases are generally performed in linear time (at least in practice, e.g. by using the simplex method for linear programming), and hence the running time is dominated by the second phase, each iteration of which requires linear time. A clarification: when we say that the running time is linear, we mean linear in the number of vertices and dummy vertices. The number of dummy vertices can be quadratic in the number of vertices—even if the graph is sparse. Nonetheless, the overall performance is generally considered sufficient to be practical.

The main drawback of the approach of Sugiyama et al. is that the layering constraints and the bends (or curves) induced by dummy vertices can cause drawings to be unaesthetic and even illegible. The approach is also somewhat inflexible, in that the aesthetic criteria are hard-wired into the algorithm.

Still, the approach of Sugiyama et al. is sufficiently effective to have become the basis for algorithms that draw directed acyclic or almost acyclic graphs. If a graph has one or more directed cycles, then a subset of the edges can be reversed to make the graph acyclic. Unfortunately, finding the minimum number of edges to reverse is NP-hard [GJ83], and reversing a large number of edges makes the flow of the drawing meaningless. There are many heuristics, the simplest being to reverse the back edges of a depth-first traversal, but none have provable performance guarantees except for dense graphs [ES90]. Also, like trees, directed acyclic graphs can be drawn on radial rather than horizontal levels [Ca80, RM88].

3.1.3. Planar Graphs

A large amount of work has considered the problem of drawing planar graphs. The key constraint is that the drawing be planar—that is, that it have no edge crossings. The published algorithms achieve this aesthetic first by testing for planarity and computing an embedding in the plane, and then transforming this embedding into a drawing. We refer the reader to the annotated bibliography [DETT94] for a listing of linear-time algorithms that test planarity and compute an embedding. For the transformation of the embedding into a drawing, the algorithms pursue various goals. Generally, edges are drawn either as straight lines or as polylines made up of only horizontal and vertical segments. Drawings with the latter kind of edges are called orthogonal drawings. Again, we refer the reader to the annotated bibliography for a fuller treatment.

3.2. Algorithms for General Graphs

Finally, we arrive at the algorithms that consider general graphs. Here, there are two schools of thought. The topology-shape-metrics approach generates orthogonal drawings of general graphs by prioritizing the aesthetics, while the force-directed approach expresses the aesthetic preferences as force laws that determine the negative gradient of an implicit objective function. We will briefly describe the topology-shapes-metrics approach for completeness, but will devote an entire chapter to the force-directed work that is more relevant to our own numerical optimization approach.

3.2.1. The Topology-Shapes-Metrics Approach

The topology-shapes-metrics approach breaks down the graph drawing process into three steps.

The first step addresses topology by planarizing the drawing—that is, determining a set of edge crossings and replacing them with dummy vertices so that the resulting graph is planar. The goal is to minimize the number of crossings; since this problem is NP-hard [GJ83], planarization algorithms use heuristics such as computing a maximal planar subgraph and then routing the remaining edges greedily. The planarization step also computes a planar embedding for the planarized graph.

The second step addresses shape by orthogonalizing the drawing—that is, assigning to each edge in the embedding an alternating chain of horizontal and vertical line segments. Here, the goal is to minimize the number of bends. Although it is NP-hard to minimize the number of bends over all possible embeddings of a planar graph [GT94], we can use a network flow algorithm to minimize the number of bends for a particular embedding in quadratic time [Ta87]. If we are more concerned with performance than with bend minimization, then we can compute a drawing with $O(1)$ bends per edge in linear time [BK94].

The third step addresses metrics by compacting the drawing so as to minimize area—subject to the embedding and edge bends computed in the previous two steps. A drawing of area $O(n^2)$ can be computed in $O(n+b)$ time [PT98].

3.2.2. The Force-Directed Approach

Force-directed algorithms, for the most part, formulate the drawing problem as one of unconstrained numerical optimization. They rely on a physically-based model, the principle aesthetic consideration being that proximity in the network should correspond to proximity in the drawing. The algorithms quantify their preferences with force laws that imply an objective function or energy. The force-directed algorithms vary mostly in their choice of force laws or their optimization strategy. Because our work is primarily concerned with drawing general graphs, we will consider the previous work here in some detail.

4. The Force-Directed Approach

Force-directed approaches use a physical analogy to model the graph drawing problem. They model the drawing as a system of forces acting on the vertices, and then aim to find a drawing where the net force acting on each vertex is zero. Equivalently, they associate a potential energy with the drawing, and seek a configuration for which this energy of the drawing is locally minimal.

Some early force-directed algorithms predate the recent interest in graph drawing per se. These include Tutte's barycenter method [Tu63] and force-directed algorithms for circuit layout [FCW67, QB79]. Here, however, we focus on more recent work that explicitly addresses the general graph drawing problem.

A *force-directed* approach consists of two components. The first is the force or energy model that quantifies the goodness of a drawing. The second is an optimization algorithm for computing a drawing that is locally optimal with respect to this model.

In this chapter, we outline the published work on force-directed graph drawing. In the following chapter, we present our own force model and compare our force laws to those used in other models.

4.1. The Spring Embedder Model

Eades published a force-directed graph drawing algorithm which he called the "spring embedder" [Ea84]. In his spring embedder model, edges act as springs acting on their endpoints with a logarithmic force law and vertices as positive electrical point charges repelling each other with an inverse-square force law. Figure 4.1 illustrates this physical model.

We note that the "forces" in this and other "force-directed" algorithms do not induce acceleration. There is no kinetic energy or momentum in the physical model; rather, each iteration reduces the potential energy of the system. As a result, the system can be described using first-order, rather than second-order, differential equations.

Eades's optimization algorithm creates an initial drawing of the graph randomly and then performs a fixed number of steepest descent iterations. On each iteration, all vertices move simultaneously in proportion to the net force exerted on them.

Eades claims that his algorithm produces good layouts for many graphs but performs poorly on dense graphs, graphs with dense subgraphs, and graphs with a small number of bridges. He also claims that his algorithm has an acceptable running time for graphs with less than fifty vertices.

Unfortunately, the vagueness of these claims makes them difficult to analyze or criticize. We can say, however, that the logarithmic spring law gives rise to an unaesthetically high degree of variance in edge length, and that some of his parameters—for example, the fixed number of steepest descent iterations—are not suitable when we increase the size of the graph. Indeed, Eades admits that he only looked at graphs of at most fifty vertices, his justification being that applications usually break up larger graphs into smaller subgraphs.

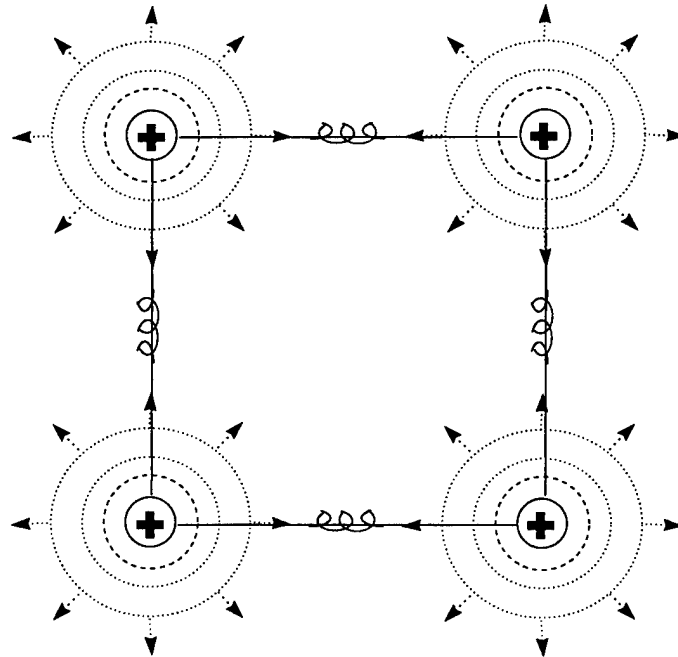


Figure 4.1: The Spring Embedder Model

4.2. Kamada and Kawai's Approach

Kamada and Kawai's approach modifies the spring embedder model by eliminating the electrical charges and instead associating a spring with every pair of vertices, rather than just with the edges [KK89]. The springs act in accordance with Hooke's Law: the force exerted on the vertices is proportional to the difference between the spring's rest length

and the actual distance between the vertices. If the actual distance is larger than the rest length, then the spring pulls the vertices closer together; if the distance is smaller, then the spring pushes them apart. For each pair of vertices, Kamada and Kawai make the spring's rest length proportional to the shortest path in the graph connecting the two vertices associated with the spring, and the spring's stiffness inversely proportional to its rest length. Kamada and Kawai conceptualize their model in terms of energy rather than forces: they integrate Hooke's Law to obtain a potential energy for each spring that is quadratic in the difference between its rest length and the actual distance between the two vertices.

Kamada and Kawai's approach also differs from that of Eades in its optimization algorithm. Rather than moving all vertices at once, their algorithm moves only one vertex in the drawing per iteration. On each iteration, the algorithm moves the vertex experiencing the greatest net force to a point of locally minimal energy using a variation of the Newton-Raphson method.

Kamada and Kawai's algorithm is not only conceptually elegant, but also produces very aesthetic drawings. The main drawback of their approach is computational: their model requires preprocessing step that computes the shortest paths for all node pairs. This computation, which requires $\theta(n^3)$ time and $\theta(n^2)$ space (see the discussion below) makes their approach impractical for large graphs.

4.3. Fruchterman and Reingold's Approach

Fruchterman and Reingold's model is similar to the spring embedder model [FR91]. It preserves the original concept of repulsive vertex charges and attractive edge springs but modifies the force laws for the sake of computational efficiency. They replace the logarithmic spring force law with one that attracts the endpoints of an edge in proportion to the square of the distance between them. Their vertex repulsion force is inversely proportional to the distance between the vertices, while Eades's model makes the repulsion inversely proportional to the square of the distance. Both of these changes reduce computation without changing the general character of the force model.

Fruchterman and Reingold's optimization algorithm, like Eades's steepest descent algorithm, uses the force laws to compute the direction in which vertices move. However, it determines the extent of their movement according to a "cooling schedule," inspired by the method of simulated annealing, that limits the distance a vertex can move

as a decreasing function of the number of iterations performed. Frick et al. address the inefficiency of Fruchterman and Reingold's cooling schedule by introducing the notion of local vertex temperatures and also attempting to detect vertex oscillation and rotation of the entire drawing [FLM94].

Fruchterman and Reingold claim that the main goals of their approach are speed and simplicity, and that the main advantage of their approach over others is the former. Like others, they do not address the problem of drawing large graphs, for which their fixed number of iterations would be insufficient. All of the examples in their paper, for which they claim that their algorithm produces drawings in less than ten seconds on a SPARC station 1, are graphs of under forty vertices. A harsher criticism of their approach, however, is that the optimization procedure is unnecessarily complicated. The cooling schedule that they use to determine how much the vertices move on each iteration is a poor substitute for a line search (which we discuss in Chapter 7); in fact, it can cause their algorithm to converge to a point that is not locally optimal.

4.4. Models that Address Edge Crossings

The force-directed models described above focus on two aesthetics: keeping edges short and distributing vertices uniformly throughout the drawing area. In Kamada and Kawai's model, one aesthetic summarizes these two: making the distance between vertices correlate to the lengths of the shortest paths connecting them in the graph. None of these models, however, takes edge crossings into account.

Two models that consider edge crossings are those of Davidson and Harel [DH96] and of Tunkelang [Tu94]. Both are energy models that include a term proportional to the number of edge crossings. Davidson and Harel use a simulated annealing algorithm for optimization, while Tunkelang uses a collection of local optimization heuristics. The discreteness of the edge crossing term rules out the continuous optimization methods used by the other force-directed approaches.

4.5. Computational Complexity

All of the force-directed approaches we have described are iterative. We therefore consider the computational complexity of performing a single iteration, as well as the number of iterations necessary to converge to a locally optimal drawing.

For the approaches of Eades, Fruchterman and Reingold, and variations thereof, the cost of performing an iteration is essentially that of computing the net force acting on every vertex. In a graph of n vertices and m edges, there are m springs and $\frac{1}{2} n (n-1)$ pairs of vertices. Hence, the cost of computing all of the forces is $\theta(n^2)$. The number of iterations necessary for convergence is poorly understood, but the consensus seems to be that a steepest descent approach requires a number of iterations that is linear in the number of vertices. Hence, the overall running time is $\theta(n^3)$.

Kamada and Kawai's approach, however, is quite different. Because it only moves one vertex per iteration, it can recompute the forces incrementally in $\theta(n)$ time. The catch, however, is in the time and space necessary for the preprocessing step of computing all shortest paths. Kamada and Kawai's algorithm performs this computation in $\theta(n^3)$ time, though this time could be reduced to $\theta(nm \log n)$ for sparse graphs by executing Dijkstra's single-source shortest paths algorithm for each vertex [CLR90]. Even for sparse graphs, however, storing the computed shortest paths requires $\theta(n^2)$ space. Kamada and Kawai claim that the number of iterations necessary for convergence is linear in the number of vertices. Hence, the overall running time is dominated by the preprocessing time.

4.6. Other Force-Directed Work

The simplicity of the force-directed approach has invited endless variations, a few of which we list here. Sugiyama and Misue use "magnetic" springs and fields that try to make edges conform to particular orientations [SM94]. Ignatowicz uses "orthogonal" springs to try to make edges meet at right angles [Ig95]. Coleman and Parker apply a variety of aesthetics to Fruchterman and Reingold's algorithm [CP96].

Two recent papers incorporate constraints into the spring embedder model. Wang and Miyamoto introduce absolute constraints on vertex position, constraints that restrict relative vertex position, and cluster constraints that cause the algorithm to treat subgraphs independently of each other [WM95]. He and Marriott allow linear constraints, as well as "suggested values" for vertex positions [HM96].

4.7. Summary of Problems in Published Approaches

The force-directed approaches of Eades and others cast the graph drawing problem into a framework of numerical optimization. Unfortunately, they do so without benefiting from the wealth of knowledge that numerical optimization offers as an established discipline.

Most of the papers of force-directed graph drawing barely even acknowledge that they are using numerical optimization as a framework. In general, they do not take sufficient advantage of results from other fields.

The most obvious flaw of the published force-directed algorithms is that they do not scale gracefully. The ever-increasing speed of hardware cannot keep up with a running time that is $\theta(n^3)$, much as cheap memory is not cheap enough for us to use an algorithm that requires $\theta(n^2)$ space. Our principle contribution to the field is to apply results from the fields of numerical optimization and many-body simulation to reduce this asymptotic running time, as well as to create an approach that meets Fruchterman and Reingold's goals of speed and simplicity.

5. Modeling Graph Drawing as an Optimization Problem

In this chapter, we formally describe the force-directed approach for modeling general graph drawing as a numerical optimization problem.

5.1. Output Variables

We denote the input graph by G . G consists of the vertex set $V = \{v_1, v_2, \dots, v_n\}$ and the edge set $E = \{e_1, e_2, \dots, e_m\}$. We denote the two endpoints of an edge e by $\text{from}(e)$ and $\text{to}(e)$. Since our edges are undirected, the ordering of the endpoints is arbitrary.

We will assume for the next few chapters that all vertices are mapped to dimensionless points and all edges to straight line segments connecting their endpoints. While we primarily intend our model for drawings in the plane, the model applies without modification to drawings in higher dimensional spaces.

We define the output variables $x(v_i)$ —or x_i for short—to be the position vectors of vertices v_i , for i equal to $1, 2, \dots, n$. For a given graph G , we denote a drawing D by the n -dimensional vector of vectors $[x_1, x_2, \dots, x_n]$. Because the edges are straight line segments, the drawing of G is completely specified by this vector of vertex positions.

5.2. Force Laws

As we described in the previous chapter, the force-directed approach models graph drawing using a physical analogy. We use a force model in which our *force laws* produce a vector that is the negative gradient of an implicit energy function we seek to minimize. There are force laws corresponding to different aesthetic criteria:

Springs. We associate a spring with each edge. A spring pulls the endpoints of the edge it represents towards each other when their distance exceeds the spring's rest length and pushes them away from each other when their distance is smaller than the rest length. If the rest length is zero, then the spring always pulls the endpoints towards each other.

Vertex-vertex repulsion. All vertices push each other away in order to avoid overlap among vertices and to spread the vertices out uniformly throughout the drawing area. The magnitude of this repulsion force for a given pair of distinct vertices is a decreasing function of the distance between the two vertices.

Vertex-edge repulsion. Vertex-vertex repulsion may not prevent a vertex from being placed so close to an edge—possibly overlapping it—that the edge appears to be incident to the vertex. Hence, we include a term in the force model for every vertex-edge pair; again, the magnitude is a decreasing function of the distance between the vertex and edge.

Although we will refer to the energy of a drawing when we discuss the numerical optimization procedure, we will mostly discuss the negative gradient of the objective function, which is the vector corresponding to the net forces on all of the vertices.

5.2.1. Springs

Since the edges specify which vertex pairs have a direct relationship, the corresponding springs serve to exhibit the importance of these relationships in the drawing.

The simplest of spring laws is Hooke's Law with a rest length of zero. Using Hooke's Law for the springs gives us, for edge e_i , a force of magnitude kx attracting each endpoint towards the other, where $x = \|x(\text{from}(e_i)) - x(\text{to}(e_i))\|$ and k is a constant representing the stiffness of the springs. We could assign a different stiffness k_i to each edge e_i to reflect the relative importance of each edge; the stiffer springs would correlate in smaller edges in an optimal drawing.

Hooke's Law (with a rest length of zero) is computationally appealing because the force vector can be computed using only one vector subtraction and one scalar multiplication. In fact, if the coordinates and spring constant(s) are integers, then the force vector can be computed exactly using only integer arithmetic.

Fruchterman and Reingold, however, found that they had more success using a quadratic spring force—that is, a force of magnitude proportional to $\|x(\text{from}(e_i)) - x(\text{to}(e_i))\|^2$. We will discuss the constant of proportionality in a moment.

Fruchterman and Reingold observed that a linear spring force is often not strong enough to overcome poor local minima—that is, local minima in the objective function that are far inferior to the global minimum. Hence, they were willing to incur the additional arithmetic operations (which include a square root) necessary for a quadratic spring force. They also experimented with using higher order powers for the spring force, but rejected them on the grounds that they were more costly to compute. In fact, a cubic spring force

would be less expensive to compute than a quadratic force, since it does not require computing a square root. We did find, however, that using higher order powers for the spring force slows down our optimization procedure by making the force laws less smooth.

Eades's original spring force for the spring embedder model was logarithmic, the magnitude of the force being proportional to $\log(\|x(\text{from}(e_i)) - x(\text{to}(e_i))\| / x_0)$, where x_0 is a user-specified constant. A fact that Eades does not mention is that this spring force becomes repulsive (rather than attractive) when $\|x(\text{from}(e_i)) - x(\text{to}(e_i))\| < x_0$. Regardless of this short-range behavior, we found, as we discussed earlier, that a logarithmic spring force leads to an unaesthetically high degree of variance in the edge lengths.

Kamada and Kawai use an model that relies exclusively on springs. Instead of only associating springs with the edges, they associate a spring with every pair of distinct vertices. Their springs conform to Hooke's Law; the rest length and stiffness of each spring depend on the length of the shortest path in the graph connecting the two vertices. If the shortest path connecting v_i and v_j has a length of $\text{shortestPath}(v_i, v_j)$ edges, then the rest length of the corresponding spring is proportional to $\text{shortestPath}(v_i, v_j)$, while the stiffness is proportional to $1/\text{shortestPath}(v_i, v_j)$. In other words, the magnitude of the spring force that each pair of distinct vertices (v_i, v_j) exert on each other is proportional to $(1 / \text{shortestPath}(v_i, v_j)) \cdot \|x_i - x_j\| - c \cdot \text{shortestPath}(v_i, v_j)$, where the constant c reflects the desired length of an edge. As Kamada and Kawai note, their model applies to graphs with either unit edges or weighted edges; in the latter case, $\text{shortestPath}(v_i, v_j)$ denotes the sum of weights along the shortest path connecting distinct vertices v_i and v_j .

As we noted in the previous chapter, Kamada and Kawai's model relies on a time and space-intensive pre-processing phase to compute and store the $\theta(n^2)$ shortest path lengths. Moreover, as we will see later, associating springs with all vertex pairs prevents us from using many-body simulation methods to reduce computation. Hence, we stick to a model of springs and repulsion.

Our own experiments agree with Fruchterman and Reingold's observation that quadratic spring force laws work better than linear springs to avoid poor local minima, and we found that using higher order polynomials for the spring laws slowed down our

optimization procedure. We therefore use Fruchterman and Reingold's quadratic spring law. In Chapter 9, we describe a modification to this law that takes vertex shape and size into account.

5.2.2. Vertex-Vertex Repulsion

If our objective function consisted only of springs of rest length zero, then the globally optimal drawing would assign all vertices to a single point. Making the rest lengths non-zero would ameliorate the situation somewhat, but edge springs alone are insufficient to produce an acceptable drawing. For example, let us consider the three-vertex path where $V = \{1, 2, 3\}$ and $E = \{(1, 2), (2, 3)\}$. A globally optimal drawing would space the vertices uniformly along a line. In the absence of a force that involves vertices **1** and **3**, these two vertices could even be assigned to identical coordinates.

As we have discussed, we reject Kamada and Kawai's solution of springs for all node pairs because of the impractical time and space requirements of the preprocessing step. Instead, we introduce vertex-vertex repulsion terms into the physical model.

In Eades's force model, vertices repel each other as if they were like-charged particles acting in accordance with Coulomb's inverse-square law. Every pair of distinct vertices v_i and v_j repel each other with a force whose magnitude is proportional to $1/\|x_i - x_j\|^2$.

When two vertices have identical coordinates, the magnitude of the repulsion force goes to infinity. We therefore disallow assignment of distinct vertices to identical coordinates. If we ever encounter a drawing where this situation occurs, we randomly separate the coincident vertices by a small distance.

Fruchterman and Reingold, concerned with reducing the number of arithmetic operations per repulsion computation and preferring to avoid taking square roots, use a force law that is inverse rather than inverse square. The magnitude of the repulsion force in their model is proportional to $1/\|x_i - x_j\|$.

Now, we can discuss the constants of proportionality in Fruchterman and Reingold's model. Fruchterman and Reingold define the constant k to denote the *rest length of an edge*. They choose their constants of proportionality for the spring and repulsion laws so that, when the length of an edge is k , then the spring and vertex-vertex repulsion forces exerted by the endpoints cancel out. In other words, two vertices joined by an edge, in

the absence of additional forces exerted on them, exert no net force when the distance between them is exactly k . When they are closer, the repulsion is stronger than the spring and pushes them apart; when they are further, the spring is stronger and pulls them towards each other.

The constants of proportionality are $1/k$ for the quadratic spring force and k^2 for the inverse vertex-vertex repulsion force. When the two endpoints of an edge are distance k apart, both forces have magnitudes of k and cancel each other out.

One issue that receives little attention in the force-directed graph drawing literature is that vertex-vertex repulsion forces serve two distinct purposes. One is to avoid vertex overlap. It is not enough that vertices be assigned distinct coordinates; since vertices are generally drawn as rectangles or ellipses with information inside them, it is preferable that they be drawn far enough apart from each other to be legible. The other purpose is to distribute vertices uniformly throughout the drawing space. This second goal is quite different from the first, and is generally a lower priority that has more to do with aesthetics—e.g., display of symmetry—than with legibility.

While the magnitude of the vertex-vertex repulsion force does decrease as a function of the distance between the vertices, the long-range effects of an inverse force law like that of Fruchterman and Reingold can be too strong, resulting in pockets of undesirably high local density. We therefore split the vertex-vertex repulsion force into a stronger short-range force and a weaker long-range force. When the distance between two vertices is less than k , we use an inverse repulsion law; when the distance exceeds k , we use a weaker inverse-square law. In order to achieve computational stability, we make the magnitude of the repulsion force continuous at k .

This way of splitting the forces is admittedly inelegant, but is a first step towards adapting the concept of vertex-vertex repulsion to address the distinct issues of avoid vertex overlap and distributing vertices uniformly.

We use the same constants of proportionality as Fruchterman and Reingold for the spring forces ($1/k$) and the short-range inverse repulsion (k^2). To achieve continuity, we use a constant of k^3 for our long-range inverse-square repulsion law.

In Chapter 9, we will discuss how node shape and size affect the vertex-vertex repulsion law. In Chapter 8, we will also discuss the computational consequences of choosing a weaker or stronger repulsion law, and how we can use a time-dependent gradient to improve performance.

5.2.3. Vertex-Edge Repulsion

In the force-directed models we have discussed, all of the forces involve vertex pairs. Sometimes these forces allow a vertex to be very close to an edge. When an edge is short, then the vertex-vertex repulsion will probably push vertices away from it. When an edge is long, however, the vertex-vertex repulsion may not prevent a vertex from being very near the edge, since it can do so without being that close to either of the endpoints.

Our concern is with vertex-edge overlap. If a vertex overlaps an edge or is placed very close to it, then it becomes difficult or impossible to determine if the edge is incident to that vertex. Hence, we need a strong short-range vertex-edge repulsion term to avoid this situation. Since we are not using vertex-edge repulsion to spread out the vertices uniformly, we do not need the force to be long-range at all. We do, however, need to make the repulsion force continuous so that we have computational stability.

We consider two cases for vertex-edge repulsion. In the first case, the point on the edge closest to the vertex is one of the endpoints. In the second case, the point closest to the vertex lies strictly between the endpoints.

In the first case, our vertex-edge repulsion force acts much like the short-range inverse vertex-vertex repulsion force acting on the vertex and the endpoint nearest to it. The only difference is that, in order to make the vertex-edge repulsion force both short-range and continuous, we subtract k from the magnitude of the force. Accordingly, the magnitude of the force is $c_{ve}((k^2/x) - k)$ when x , the distance between the vertex and the closer endpoint, is less than k (we will discuss c_{ve} in a moment). This force pushes the vertex and the endpoint closest to it away from each other; it does not affect the further endpoint. Indeed, it only amplifies the vertex-vertex repulsion force that the two vertices already exert on each other. We need this force, however, to ensure continuity with the second case.

The second case is more complicated. First, we compute the distance x between the vertex on the edge by projecting the former onto the latter. Let us denote the vertex by v ,

the edge by \mathbf{e} , and the projection of \mathbf{v} onto \mathbf{e} (that is, the point on the edge closest to \mathbf{v}) by \mathbf{p} . Let $\alpha = \|\mathbf{p} - \mathbf{x}(\text{from}(\mathbf{e}))\| / \|\mathbf{x}(\text{to}(\mathbf{e})) - \mathbf{x}(\text{from}(\mathbf{e}))\|$. By assumption, $\alpha \in [0, 1]$; the boundary situations ($\alpha = 0$, $\alpha = 1$) represent the first case, where the point on the edge close to \mathbf{v} is an endpoint.

We can now describe the vertex-edge repulsion force law for the second case. Vertices \mathbf{v} and $\text{from}(\mathbf{e})$ repel each other with a force of magnitude $(1-\alpha)\mathbf{c}_{ve}((k^2/x)-k)$. Symmetrically, vertices \mathbf{v} and $\text{to}(\mathbf{e})$ repel with a force of magnitude $(\alpha)\mathbf{c}_{ve}((k^2/x)-k)$. As we can see by setting α to 0 or 1, the boundary cases are continuous.

The constant \mathbf{c}_{ve} is a non-negative weight that reflects the priority of avoiding vertex-edge overlap. We have found that a small value of \mathbf{c}_{ve} works well; our own implementation sets it to 0.1.

5.3. Constraints

Constraints can be either equalities or inequalities in the output variables. A drawing that satisfies all of its constraints $\mathbf{C}_1, \mathbf{C}_2, \dots$ is said to be *feasible*, and the set of such drawings is said to be the *feasible space* of drawings. If the set of constraints is empty, then all drawings are feasible, and the problem is said to be *unconstrained*.

5.3.1. Penalty Functions

For every constraint \mathbf{C}_i , we will require an associated *penalty function* \mathbf{p}_i that measures the distance of a drawing to the nearest drawing that satisfies \mathbf{C}_i . We can define such penalty functions for both equality and inequality constraints. The requirement that these penalty functions exist allows us to use the method of exterior penalties to perform constrained optimization. We will describe this method in Chapter 8.

5.3.2. Constraints versus Preferences

It is often possible to quantify aesthetic criteria either as constraints or as terms in the objective function. In the latter case, the criteria become preferences that are combined and prioritized according to their relative weights. The choice of whether to represent an aesthetic criterion with constraints or preferences is key to the modeling problem, so we will discuss the advantages and disadvantages of each type of formulation.

For example, we may have two vertices that are very strongly related. A simple way to express the strength of their relationship in the drawing is to constrain them to lie within a

certain distance of each another. Alternatively, we could represent this strength using a spring term in the objective function with a high spring constant.

The main advantage of constraints is their simplicity. If we have non-negotiable aesthetic criteria and can express them as boolean predicates, then constraints provide a straightforward mechanism for doing so. Typical constraints address minimal separation between nodes, drawing boundaries, clustering, and edge direction.

Constraints, however, have two major disadvantages. First, their binary nature limits their expressiveness. In the example above, we can use constraints to specify a minimum node separation, but our formulation does not favor larger distances over small ones. The second problem is more serious: they generally add complexity to the optimization process and thus slow it down. Here, we must accept that there is a trade-off between speed and flexibility.

6. Computing the Gradient Efficiently

The $\theta(n^3)$ running time of most of the published graph drawing algorithms effectively limits their domain to very small graphs. To draw larger graphs, we must dramatically reduce the running time.

In this chapter, we focus on making the computation of the gradient as efficient as possible. In particular, we attack the bottleneck of the published force-directed approaches—the $\theta(n^2)$ computation of repulsion forces. After discussing two simple but problematic methods that reduce this computation to $\theta(n)$, we discuss more sophisticated approaches drawn from the many-body simulation literature.

6.1. Computing the Gradient Naïvely

In order to compute the gradient of a drawing as we defined it in the previous chapter, we need to take a sum of $\theta(m)$ spring forces, $\theta(n^2)$ vertex-vertex repulsion forces, and $\theta(nm)$ vertex-edge repulsion forces. Even without considering vertex-edge repulsion forces, we would require $\theta(n^2)$ time to compute the gradient straightforwardly—that is, by summing all of the spring and vertex-vertex repulsion forces to compute the net force acting on each vertex.

A running time of $\theta(n^2)$ or $\theta(nm)$ for a single gradient computation severely limits the size of graphs that we can draw. For dense graphs—that is, where m is $\theta(n^2)$ —we have little hope of doing better unless we can somehow summarize the graph in a smaller representation. For example, we could take a divide-and-conquer approach that partitions the vertices into subsets, draws each subset independently, and then draws the graph of subsets as if each subset were a single large vertex. This partitioning problem, however, is beyond the scope of this dissertation. We thus assume we cannot avoid computing the spring forces, and this computation requires $\theta(m)$ time.

For sparse graphs, however, there is a wide gap between $\theta(m)$ and $\theta(n^2)$. Indeed, for sparse graphs, we spend most of the computation on the repulsion forces—that is, assuming that we compute these forces naïvely. Accordingly, we devote our efforts to computing these repulsion forces more efficiently.

6.2. Simple $\theta(n)$ Approximations for Computing Vertex-Vertex Repulsion

In the force-directed graph drawing literature, two techniques appear for approximating the computation of the vertex-vertex repulsion forces. Fruchterman and Reingold describe a “grid variant” of their algorithm that ignores repulsion forces between vertex pairs whose distance exceeds a threshold of $2k$, using an auxiliary grid structure to reduce computation. As we discussed in the previous chapter, k is the rest length of an edge—that is, the distance at which the two endpoints of an edge exert no net force on each other because the spring and repulsion forces cancel out. Fruchterman and Reingold claim that this approximation produces drawings that are “nearly equivalent” to those obtained without approximation. They note that this approximation of the repulsion forces has a running time that is $\theta(n)$ when the vertex distribution in the drawing area is “approximately uniform”; the efficiency of their grid structure depends on the uniformity of the distribution. Coleman and Parker suggest the alternative approach of “centripetal repulsion”—that is, repulsion from the centroid of the drawing. The cost of this approximation is $\theta(n)$ time (and no additional space) regardless of the distribution of vertices.

6.2.1. Distance Cut-Offs

Distance cut-offs are a conceptually simple approach to approximating vertex-vertex repulsion. Since the magnitude of the vertex-vertex repulsion forces decays rapidly with distance between the two vertices, we can ignore repulsion between far-away vertices and only incur a small additive error in the gradient. Moreover, we can implement distance cut-offs, as Fruchterman and Reingold do, with a straightforward data-structure: we partition the drawing space uniformly into a grid of square cells where the side of each square is the cut-off distance. Fruchterman and Reingold choose their constants so that k^2n is proportional to the area of the drawing space, making the number of grid cells—and hence the additional space required for the grid— $\theta(n)$.

We can easily determine a bound on the maximum additive error caused by using distance cut-offs. In Fruchterman and Reingold’s force model, the magnitude of the repulsion force between nodes v_i and v_j is $k^2 / \|x_i - x_j\|$. When $\|x_i - x_j\| = 2k$, this force has a magnitude of $k/2$. Hence, the maximum additive error in computing the magnitude of each repulsion force is $k/2$.

While the additive error resulting from distance cut-offs is small, they are unsatisfactory for two reasons. The first is basic: by ignoring long-distance repulsion forces, we inhibit

most of the effect that vertex-vertex repulsion would normally have in distributing the vertices uniformly throughout the drawing space. The second is that distance cut-offs cause problems for the optimization procedure. In Fruchterman and Reingold's model, the cut-offs make the force model discontinuous wherever the distance between two vertices is exactly $2k$, since the magnitude of the repulsion force jumps from $k/2$ to 0 . Such discontinuities can cause an optimization procedure to oscillate around them. We can remove the discontinuities using the technique we applied to our short-range vertex-edge repulsion force—that is, we can make the magnitude of the vertex-vertex repulsion force $k^2 / \|x_i - x_j\| - k/2$ so that it is continuous at $\|x_i - x_j\| = 2k$. Fruchterman and Reingold's algorithm handles the discontinuities by dampening forces using a "cooling schedule", but there is no guarantee that the drawing to which it converges will be locally optimal.

We can lessen the consequences of distance cut-offs by increasing the cut-off distance. Assuming that the graph is connected, there always exists a cut-off distance that has no effect on the objective function—namely, any value greater than the diameter of the optimal drawing. Doing so, however, defeats the entire purpose of the approximation, which is to reduce computation.

Indeed, the efficiency of Fruchterman and Reingold's grid variant hinges on the assumption that the number of vertices within the cut-off radius of a vertex is, on average, $\theta(1)$. If we further assume a uniform distribution of vertices in the drawing space, then this requirement implies a $\theta(k)$ cut-off distance, since the expected number of vertices within a cut-off radius of r is $\theta(r^2/k^2)$. As a result, modifying the grid variant to use a cut-off distance of r increases the running time (assuming uniform vertex distribution) to approximately compute repulsion forces from $\theta(n)$ to $\theta(r^2n/k^2)$, where r is at most $O(k\sqrt{n})$. If r is greater, then we may as well use the naïve $\theta(n^2)$ approach.

The assumption that the vertex distribution will be "approximately uniform" is, however, somewhat questionable. As shown in Figure 6.1, a cycle of n vertices with edges of length k requires a drawing area of $\theta(k^2n^2)$ to be drawn as a regular polygon—which is accepted as the optimal way to draw an undirected cycle. Fruchterman and Reingold's grid variant can handle this situation in a few ways. One possibility is to impose a drawing space of area $\theta(k^2n)$, in which case the boundary will severely constrain the drawing. If the area of drawing space is $\theta(k^2n^2)$, then there is the question of choosing the number of grid cells. If there are $\theta(n)$ grid cells, then, as the drawing approaches its optimum, each of the $\theta(\sqrt{n})$ cells on the perimeter will contain $\theta(\sqrt{n})$ vertices, making the

total running time to compute repulsion forces $\theta(n^{1.5})$. In order to reduce the average number of vertices in a non-empty cell to $\theta(1)$, we would have to use $\theta(n^2)$ cells—bringing the running time up to $O(n^2)$.

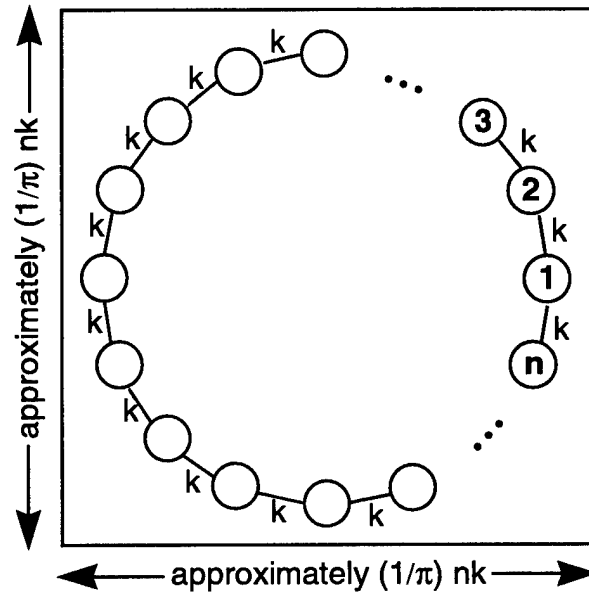


Figure 6.1: Cycles have highly non-uniform vertex distribution

Finally, although we can use distance cut-offs for drawings in higher-dimensional spaces, we can only do so efficiently if the vertex distribution is approximately uniform in the space. In any space, distance cut-offs only give us an efficient procedure if the drawing occupies $\theta(n)$ grid cells and the average number of vertices in each non-empty cell is $\theta(1)$.

6.2.2. Centripetal Repulsion

An alternative approach to approximating the vertex-vertex repulsion forces is to replace them by a repulsion from the centroid of the drawing. As Coleman and Parker point out, centripetal repulsion can sometimes work as a substitute for vertex-vertex repulsion.

Our notion of centripetal repulsion is slightly but significantly different from that of Coleman and Parker. We see centripetal repulsion as an extreme case of monopole approximation—that is, we consider a vertex's interaction with the $n-1$ other vertices as if the latter were consolidated into a single large vertex at their centroid. Hence, we

modify Coleman and Parker's approach in two ways. First, vertices experience repulsion from the centroid of the $n-1$ other vertices, rather than from the centroid of all n vertices in the drawing. Second, the repulsion force is mutual—that is, the centroids are also repelled by the vertices. This latter modification ensures that the sum of all repulsion force vectors in the drawing always cancels out, and hence that the centroid of the drawing will not drift. Like distance cut-offs, centripetal repulsion generalizes to drawings in higher dimensional spaces.

Centripetal repulsion has several immediate advantages over distance cut-offs. The time necessary to compute all of the centripetal repulsion forces is $\theta(n)$ regardless of the vertex distribution, and there is no need to maintain an auxiliary grid data structure. Centripetal repulsion does not suffer from the discontinuities of distance cut-offs; in fact, the further a vertex is from the centroid of its neighbors, the more accurate the approximation. Also, for drawings in higher dimensional spaces, the cost of computing centripetal repulsion only increases linearly with the number of dimensions. Indeed, it is a more elegant model, both in concept and in the implementation.

Unfortunately, its inaccuracy can be far more severe than that of distance cut-offs. Let us consider the 15-vertex binary tree drawn optimally in Figure 6.2. Using centripetal repulsion, we obtain the bizarre drawing in Figure 6.3. Because vertices don't repel each other directly, it is even possible for them to be assigned to identical coordinates. A smaller but still significant problem with centripetal repulsion is that it distorts the drawing near its centroid.

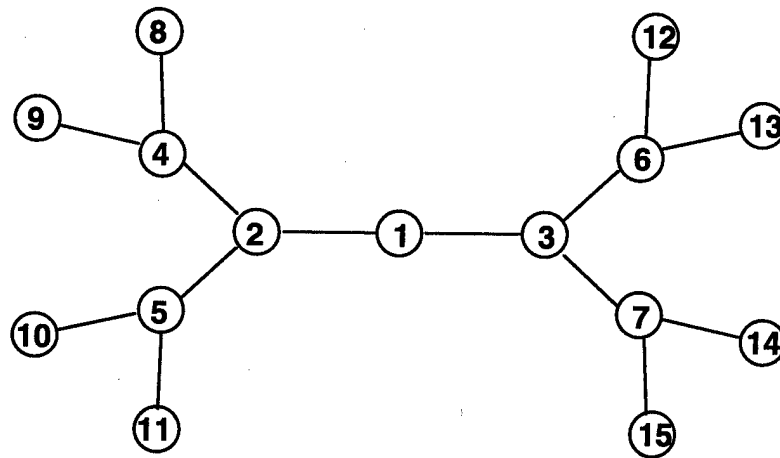


Figure 6.2: Optimal Drawing of Tree

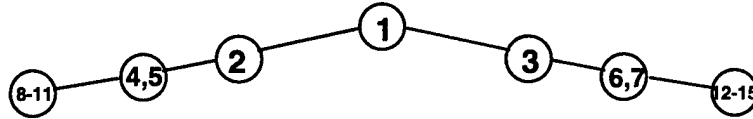


Figure 6.3: Same Tree Drawn using Centripetal Repulsion

We might address this problem by combining distance cut-offs with centripetal repulsion, but this approach would be messy. It would also suffer from the problems of both approaches—for example, degradation in speed when the vertex distribution is not close to uniform, and distortion near the centroid. Instead, we turn to the many-body simulation literature for a better solution.

Interestingly, the two approaches we have discussed, distance cut-offs and centripetal repulsion, demonstrate the two distinct purposes of the vertex-vertex repulsion force. Distance cut-offs focus only on the short-range repulsion for avoiding overlap, while centripetal repulsion helps make the vertex distribution more uniform. As we will see, we can accomplish both of these goals by combining our distinction between short- and long-range repulsion with an efficient tree-code.

6.3. Approximating Vertex-Vertex Repulsion Forces in $\theta(n \log n)$ Time

The problem of computing the pair-wise interactions among a large collection of particles is a familiar one to physicists. Indeed, their methods for approximating gravitational and electrostatic forces are directly relevant to our problem.

Two popular procedures to compute this approximation are Greengard and Rokhlin's Fast Multipole Method (FMM) [GR87] and the Barnes-Hut algorithm [BH86]. Both rely on partitioning the set of particles hierarchically into a tree of cells. Barnes-Hut replaces most particle-particle interactions with particle-cell interactions, while FMM computes a series of cell-cell interactions. Although worst-case running-time of FMM is asymptotically better than that of Barnes-Hut— $\theta(n)$ versus $\theta(n \log n)$ —it has much more overhead and is also more complicated to implement. The performance and accuracy of Barnes-Hut are more than adequate for our purposes.

We now describe how the Barnes-Hut algorithm works for particles in two dimensions. The algorithm consists of two phases. In the first, we partition the drawing space by creating a quad-tree of rectangular cells. In the second, we traverse the quad-tree to

approximate the net force acting on each particle. The algorithm generalizes to spaces of higher dimension, and is commonly applied to problems in three dimensions.

6.3.1. Building the Quad-Tree

In the first phase, we insert all of the particles into a quad-tree. A *quad-tree* is a hierarchical partitioning of a rectangle, where each internal node of the tree represents a rectangle that has been split into four congruent subrectangles (i.e. bisected horizontally and vertically) and each leaf is an undivided rectangle. We refer to both internal nodes and leaves of the quad-tree as *cells*.

We begin with a single empty cell that represents the bounding rectangle of the particles. If we do not already know the bounding rectangle, we can compute it in $\theta(n)$ time, where n is the number of particles.

We then insert the particles into the quad-tree sequentially. When we insert a particle, we begin at the root of the quad-tree. We increment the number of particles stored in that cell by one, and also update that cell's centroid. If the cell was empty, then its centroid is the position of the inserted particle; otherwise, we take a weighted average of the previous centroid and the new particle's position. Now there are three cases. If the cell was an empty leaf, then we are done with the insertion. If the cell is an internal node, we recursively insert the particle into the subcell corresponding to the rectangle that contains the particle. If the cell was a leaf that already had a particle in it, then we make the cell an internal node, splitting it into four subcells. We then recursively insert both of the cell's particles into the appropriate subcells.

Figure 6.4 illustrates how we partition the bounding rectangle of the particles into cells such that each cell contains at most one particle. Figure 6.5 shows a quad-tree that represents this partitioning. The children of a cell represent, in order, the northwest, northeast, southwest, and southeast quadrants of that cell.

Our insertion procedure maps each particle to a unique leaf in the quad-tree. There are also empty leaves in the tree—possibly as many as three for each internal node of the tree. In total, the space requirement for the quad-tree is $\theta(n)$.

The time required to create the quad-tree depends on its height. Inserting a particle requires time proportional the distance from the root to the leaf that contains that particle.

is a constant lower bound on the smallest distance between particles. We can also assume that s is $O(n)$, the bounding case being a path of n vertices drawn along a straight line. Hence, each leaf has an area that is at least $\Omega(1/n)$ fraction of the area of the bounding rectangle. This lower bound implies that the height of the quad-tree is $O(\log n)$, making the time to create it $\theta(n \log n)$.

6.3.2. Computing the Force on Each Particle

The performance gain in the Barnes-Hut algorithm comes from computing the force exerted on a particle by other far-away particles with a monopole approximation—that is, treating collections of particles as if they were clustered at their centroids. We do have to take care, however, not to make gross errors using this monopole approximation.

The procedure for computing the force acting on a particle works as follows. We first find the leaf cell of the quad-tree associated with that particle. We then compute the force exerted by each of that cell's siblings on the particle. When then take the leaf's parent in the tree and compute the force exerted by each of the parent's siblings on the particle. We do the same with the parent's parent, and so forth, until we reach the root.

How we compute the force that a cell exerts on the particle depends on whether the leaf cell containing the particle is well separated from the cell. Barnes and Hut define this concept as follows: a particle and a cell are *well separated* if the ratio r/D is less than θ , where r is the length of a side of the cell, D is the distance between the particle and the centroid of the cell, and θ is a fixed accuracy parameter between zero and one. We will discuss the choice of θ in a moment.

If a particle is well separated from a cell, then we compute the force exerted by the cell as if all of its particles were located at the centroid of the cell. Otherwise, we recursively compute the force exerted by each of the subcells of that cell on the particle.

The reason for insisting that cells be well separated for the monopole approximation is that using centroids for cells that are not well separated can result in unbounded errors. Two particles that are very close to each other may end up in leaf cells that share a border but are nonetheless far apart from each other in the quad-tree.

Barnes and Hut suggest setting θ to be approximately 1. Salmon has shown the total number of force computations necessary is $O(\theta^{-3} n \log n)$ [Sa90], and that the errors in

the force computation can be unbounded if $\theta \geq d^{-1/2}$, where d is the number of dimensions of the space [SW94]. If $d = 2$, we must pick $\theta < 0.707$. We have had good results with $\theta = 0.7$ is more than sufficient. In particular, our algorithm does not suffer from the discontinuities introduced by reorganizing the quadtree as vertices move in the drawing.

We should note that the above error analysis assumes that the force law is an inverse-square law, as is the case in gravitation and electrostatics. In practice, we have found that the Barnes-Hut algorithm works even when the force law is inverse. In any case, our long-range repulsion force is inverse-square.

We conclude this section with an example: we use the Barnes-Hut algorithm to compute the force acting on particle **1** in Figure 6.4.

The siblings of the associated leaf cell are the leaf cell containing particle **8**; the non-leaf cell containing particles **2**, **3**, and **4**; and the leaf cell containing particle **10**. The computation is trivial for the two siblings that are leaves; we just compute the ordinary particle-particle forces.

The non-leaf sibling requires more work. Since it is not well separated from the leaf cell containing particle **1**, we have to compute the forces that its children exert on particle **1**. The non-empty children are the non-leaf cell containing particles **2** and **4**, and the leaf cell containing particle **3**. Again, the leaf cell computation is trivial, but again the non-leaf cell is not well-separated from the leaf containing particle **1**. Hence, we look at its non-empty children, which are both leaves.

Now, we look at the siblings of the parent of the leaf cell containing particle **1**. These are the non-leaf cell containing particles **5**, **6**, **7**, **9**, and **11**; the leaf cell containing particle **14**; and the non-leaf cell containing particles **12**, **13**, and **15**. Finally, we see how the quad-tree helps: both of the non-leaf cells are well separated from the leaf cell containing particle **1**. Hence, we compute the force that each exerts in constant time by treating each cell as if all of its particles were at its centroid.

Since the parent of the parent of the leaf cell containing particle **1** is the root of the quad-tree, we are done.

6.3.3. Applying Barnes-Hut to Compute Vertex-Vertex Repulsion Forces

The vertex-vertex repulsion in our physical model considers a particle system like those that Barnes and Hut had in mind for their algorithm. Our force law does not correspond exactly to the physical laws of gravitation or electrostatics; nonetheless, the Barnes-Hut algorithm works very well to approximate it.

We do however, make one minor modification. As we discussed in the context of centripetal repulsion, we would like the net force on the centroid of the drawing to be zero, since all of the forces should cancel each other out. Unfortunately, the Barnes-Hut algorithm does not make us such a guarantee. We address this problem much the way we did for centripetal repulsion: we make all forces mutual. In other words, a particle exerts a repulsion force on a cell equal in magnitude to the force that the cell exerts on the vertex. If the cell contains c vertices, then each of the vertices experiences $1/c$ of this force.

6.4. Computing Vertex-Edge Repulsion Forces

We could also modify the Barnes-Hut algorithm to compute vertex-edge repulsion. The modifications, however, would not be trivial: we would have to break up the line segments representing edges into sub-segments such that each leaf cell of the quad-tree would contain at most one sub-segment. The quad-tree would require a space proportional to the number of sub-segments, which could be somewhat larger than the number of edges. In addition, we would have to take more care with the force computation, since the three cases for vertex-edge repulsion are more complicated than the single law for vertex-vertex repulsion.

A key difference, however, between vertex-vertex and vertex-edge repulsion is that the latter is a purely short-range force. Using Barnes-Hut is overkill, since we lose no accuracy by ignoring vertex-edge pairs that are far apart. In fact, we can use distance cut-offs, taking an approach based on Fruchterman and Reingold's grid variant.

Like Fruchterman and Reingold, we partition the bounding rectangle of the drawing space into a grid of square cells such that the side of each cell is k and store in each cell a list of the vertices it contains. If the vertex distribution is sufficiently uniform, then the number of cells will be proportional to the number of vertices; otherwise, we can use a sparse matrix representation in which non-empty cells do not take up memory.

Once we have computed the grid, we iterate over the edges, computing the repulsion force between it and the vertices that are near it. An edge may not be entirely contained in one cell, in which case we have to iterate over all of the cells it occupies. Indeed, the vertices we have to consider are precisely those that are either in the cells occupied by the edge or are in cells that border those occupied by the edge. If an edge is of length $O(k)$, then it will occupy $O(1)$ cells.

Unlike Fruchterman and Reingold, we do not have to contend with the inaccuracy caused by using distance cut-offs. Our vertex-edge repulsion force is short-range by design, so there is no inaccuracy.

We do, however, suffer the same performance problems that they do if the vertex distribution is highly non-uniform. One heuristic to address this issue is to ignore vertex-edge repulsion in the early iterations. By doing so, we solve several problems. By the time we start computing vertex-edge repulsion, the vertex distribution corresponds roughly to what it will be in the final drawing. Waiting until later iterations to introduce vertex-edge repulsion also helps us avoid poor local minima. If, after a large number of iterations, there are still edges with large numbers of vertices within distance k of them, then we must resign ourselves to the fact that the drawing is dense and requires more work. In practice, the number of vertices within distance k of an edge is $O(1)$, making the time to compute vertex-edge repulsion forces $O(m)$.

7. The Optimization Procedure

So far, we have concerned ourselves only with the efficiency of computing the gradient. The other factor that determines performance is the number of gradient computations that our optimization procedure must perform before converging to a local minimum.

As we discussed in Chapter 4, we can think of the graph drawing problem in terms of either a force model or an energy model. In the previous chapter, we opted for the former, describing how we encapsulate the aesthetic criteria with force laws. Now it proves convenient to imagine the sum of these force vectors as the negative gradient of an energy function that we are trying to minimize. We refer to this implicit energy function as the objective function.

We restrict our attention to first-order continuous optimization procedures. Such procedures are iterative: on each iteration, they improve the drawing (which is a vector in \mathbb{R}^{2n} for two-dimensional drawings), translating it by some vector $\mathbf{p} \in \mathbb{R}^{2n}$. We break down the problem of computing this vector into two sub-problems: that of choosing a *search direction*—that is, the orientation of \mathbf{p} —and that of determining the *step size*, the magnitude of \mathbf{p} .

The algorithms of Eades and of Fruchterman and Reingold use variations of the method of steepest descent. Accordingly, we first discuss this straightforward method for choosing the search direction. We then describe how to compute the search direction using the conjugate gradient method. Finally, we discuss the problem of computing the step size.

7.1. The Method of Steepest Descent

The method of *steepest descent*, also known as Euler's Method in the context of solving differential equations, uses the negative gradient as the search direction. In the context of force-directed graph drawing algorithms, moving along the negative gradient simply means moving each vertex in the direction of the net force exerted on it.

Eades's optimization procedure uses the method of steepest descent as is. Fruchterman and Reingold start by computing the negative gradient, but then, instead of computing a step size, they truncate each vertex's components of the search direction independently in

order to limit the maximum distance that a vertex can move on that iteration. They determine this maximum distance according to a “temperature” that is a decreasing function of the number of iterations performed thus far.

The main selling point of the method of steepest descent is its simplicity. It allows us to compute a search direction with only one gradient computation. Moreover, as long as we take some care in choosing the step size and have sufficient numerical precision, the method of steepest descent will always converge to a local minimum, regardless of our starting point.

Unfortunately, although the method of steepest descent does eventually converge to a local minimum, it may take a large number of iterations to do so. We can make this statement more formally for the case that the objective function is *quadratic* and *positive definite*—that is, its Hessian matrix of second derivatives is constant and has only positive eigenvalues. In this case, the method of steepest descent is only guaranteed to converge at a rate that is linear in the *condition number* of the Hessian, which is defined as the ratio between the smallest and largest of its eigenvalues. We refer the reader to Gill, Murray, and Wright [GMW81] for a thorough analysis of the convergence rate of the method of steepest descent.

In our own case, the objective function is neither quadratic nor positive definite; nonetheless, the method of steepest descent slows down when the condition number of the Hessian is large.

By always following the negative gradient, the method of steepest descent models the local behavior of the objective function as linear. Since non-degenerate linear functions do not even have local minima, this model is obviously a crude one. While the method of steepest descent performs reasonably well when we are far away from a local minimum—where the objective function behaves most linearly—its performance degrades rapidly as we approach the local minimum.

Often, the method of steepest descent will find itself stuck in a “trough,” a situation we depict in Figure 7.1. The little black arrows in the figure indicate the direction of the negative gradient, which each of the thick gray arrows indicates the progress on a single iteration. Let us assume that we are using the maximum possible step size that will

decrease the objective function. In that case, the method of steepest descent will bounce back and forth, making very slow progress.

In order to do better than the method of steepest descent, we need a more sophisticated model of the objective function.

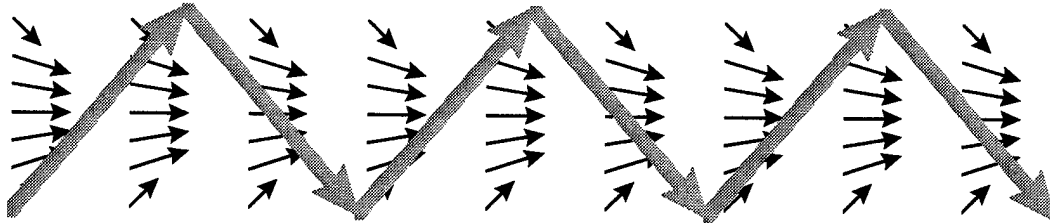


Figure 7.1: Steepest Descent Makes Slow Progress in a Trough

7.2. The Newton Direction

The method of steepest descent is based on a linear model of the objective function—that is, a model in which the gradient at each iteration is treated as a constant. We now consider an approach that uses a quadratic model of the objective function. Most of the following discussion paraphrases that of Gill, Murray, and Wright [GMW81].

We construct this quadratic model by taking the first three terms of the Taylor series of the objective function about the current drawing. We denote the objective function by F , the current drawing by D , the gradient vector by F' , and the Hessian matrix of second derivatives by F'' . The first three terms of the Taylor series give us the following expansion:

$$F(D + p) = F(D) + F'(D) \cdot p + \frac{1}{2} p \cdot F''(D)p,$$

where p is the displacement from the current drawing.

Since we are assuming that the Hessian $F''(D)$ is constant, we will denote it by H . If H is positive definite, then there is a unique global minimum that we can obtain by minimizing the following quantity Φ with respect to p :

$$\Phi(p) = F(D + p) - F(D) = F'(D) \cdot p + \frac{1}{2} p \cdot (Hp)$$

Finding the minimum of Φ is, in turn, equivalent to solving the linear system of equations:

$$\mathbf{H}\mathbf{p} = -\mathbf{F}'(\mathbf{D})$$

The value of \mathbf{p} that solves this linear system is called the *Newton* direction.

We could solve this linear system of equations to obtain the Newton direction. Unfortunately, we would need $\mathbf{O}(n^2)$ time and space just to compute \mathbf{H} , let alone to solve the system. What we would like is a faster technique that approximately follows the Newton direction without requiring us to compute \mathbf{H} .

7.3. The Conjugate Gradient Method

In order to achieve the effect of following the Newton direction without actually computing \mathbf{H} , we turn to the conjugate gradient method. The *conjugate gradient* method is an iterative technique that computes the Newton direction for a quadratic function whose Hessian is positive definite. We first discuss the conjugate gradient method for quadratic, positive definite functions and then generalize it to handle more general functions.

We define a collection of linearly independent vectors $\mathbf{p}_0, \mathbf{p}_1, \mathbf{p}_2, \dots$ to be our *search directions* and define \mathbf{P}_i to be the vector space spanned by $\mathbf{p}_0, \mathbf{p}_1, \mathbf{p}_2, \dots, \mathbf{p}_i$. We will discuss how to compute these vectors in a moment. We also have a collection of vectors $\mathbf{x}_0, \mathbf{x}_1, \mathbf{x}_2, \dots$ that represent successive approximations to the location of the minimum of Φ . We define \mathbf{x}_i to be the vector that minimizes Φ over the manifold \mathbf{P}_i . Hence, for a problem of $2n$ independent variables, \mathbf{x}_{2n} is the true minimum of Φ , since $\mathbf{P}_{2n} = \mathbf{R}^{2n}$. Finally, we define a sequence of gradients $\mathbf{g}_0, \mathbf{g}_1, \mathbf{g}_2, \dots$ such that $\mathbf{g}_i = \nabla \Phi(\mathbf{x}_i)$.

By choosing the search directions to be *mutually conjugate* with respect to \mathbf{H} —that is, so that they satisfy the condition $\forall i, j$, such that $i \neq j$: $\mathbf{p}_i \bullet (\mathbf{H}\mathbf{p}_j) = 0$ —we obtain the simplification: $\mathbf{x}_{i+1} = \mathbf{x}_i + \alpha_i \mathbf{p}_i$, where $\alpha_i = -(\mathbf{g}_i \bullet \mathbf{p}_i) / (\mathbf{p}_i \bullet (\mathbf{H}\mathbf{p}_i))$. Instead of using \mathbf{H} to compute α_i , we can, as we will discuss in section 7.5, find it with a line search.

The remaining question is how we choose the search directions. We set \mathbf{p}_0 to be the direction of steepest descent. We obtain the remaining vectors as follows:

$$\mathbf{p}_k = -\mathbf{g}_k + (\|\mathbf{g}_k\| / \|\mathbf{g}_{k-1}\|)^2 \mathbf{p}_{k-1}$$

A proof that these search directions are mutually conjugate can be found in Gill, Murray, and Wright's text [GMW81].

Assuming that the objective function is quadratic, its Hessian is positive definite, and the line search is exact, then we obtain an exact minimum in at most $2n$ conjugate gradient iterations.

To get an intuition for how the conjugate gradient method outperforms steepest descent, let us return to the example in Figure 7.1. As we can see from the picture, $\|g_1\| / \|g_0\|$ is approximately 1. For simplicity, we will assume that the magnitudes of both gradients are identical. In that case, the second iteration, rather than following the negative gradient g_1 , uses as its search direction (shown with a thick black line) $p_1 = -(g_0 + g_1)$. This summation, as we can see in Figure 7.2 cancels out the vertical oscillation that slows down steepest descent, allowing us to escape from the trough in only two iterations. While this example is unrealistically simple, it does provide an intuition for why the conjugate gradient method significantly outperforms steepest descent.

For a quadratic, positive definite objective function, the conjugate gradient method has rate of convergence proportional to the square root of the condition number of the Hessian (as compared to steepest descent, which is linear).

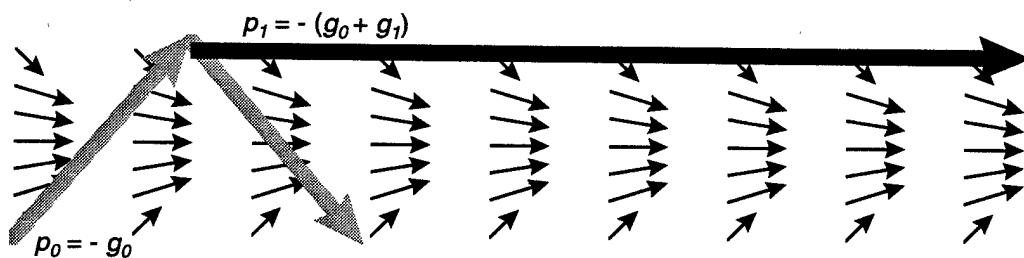


Figure 7.2: The Conjugate Gradient Method Escaping a Trough

7.4. The Conjugate Gradient Method with Restarts

Unfortunately, some assumptions that we made about the objective function do not, in fact, hold. The objective function is not quadratic; the Hessian may not be positive definite; and an exact line search is impractical. Moreover, we have no desire to perform $2n$ conjugate gradient iterations, since $2n$ conjugate gradient iterations would require $\theta(nm + n^2 \log n)$ time.

In light of these issues, we modify the conjugate gradient method by *restarting* it whenever the search direction is not a descent direction, i.e. its dot product with the gradient of the objective function is non-negative.

While this heuristic undermines theoretical claims about our method, experiments show it to be a significant improvement over the method of steepest descent. We will present an empirical comparison between the conjugate gradient method with restarts and the method of steepest descent in Chapter 11.

7.5. Computing the Step Size

Whatever our method for choosing the search direction, we need a procedure that computes an admissible step size. We refer to such a procedure as a *line search*, since it searched along the line defined by the search direction. We define a step size to be *admissible* if it satisfies the following criteria:

- 1) It is positive.
- 2) It causes the objective function to decrease.
- 3) The angle between the new gradient (after moving the drawing) and the old gradient has an angle greater than or equal to some constant γ , where $0 < \gamma \leq \pi / 2$.

The first criterion simply enforces the search direction; we are interested in moving along the search direction, not opposite to it. The second criterion prevents us from taking steps that are too large, and ensures that each iteration of the optimization procedure will actually improve the drawing. Finally, the third criterion prevents us from taking steps that are too small. The value of γ determines the accuracy of the line search: a larger value corresponds to a more accurate search. We set $\gamma = \cos^{-1}(0.5)$ in our implementation. As long as the step size satisfies these three properties, then we will converge to a local minimum.

To compute an admissible step size, we first *bracket* the step size—that is, determine a finite interval that contains an admissible step size. Since we already have zero as the lower bound of the interval, we only have to compute an upper bound. We make a guess, and then keep doubling it until either it is an admissible step size or the dot product between the gradient obtained after using it as a step size and the old gradient is negative.

In the latter case, we have to search the interval to find an admissible step size; we can do so using bisection, polynomial interpolation, or other line search techniques.

An *exact* line search finds a stationary point along the search direction—that is, a point where the gradient is orthogonal to the present one. The benefits of using an exact line search, however, do not justify the amount of computation necessary to find the stationary point. In fact, we are ultimately limited by the floating point precision of the machine. But it is not even practical to perform a particularly accurate line search, since our overall computational cost is proportional to the number of gradient computations performed per line search.

Eades takes the simplest approach: he uses a fixed step size. Unfortunately, there is no guarantee that this step size is admissible. In particular, if it is too large, the optimization may oscillate and never converge to a local minimum.

Our experiments showed, however, that a fixed step size often does very well in practice. In fact, most of our sophisticated line search approaches slowed us down by increasing the number of gradient computations per iteration. Determined to keep this number small, we decided to compute the step size adaptively.

When we start our computation, we initialize the step size to be one. On each iteration, we check if the current step size is admissible. If it is, we use it. If it is too small—that is, if the angle between the gradient after taking the step and the current gradient is closer to zero than an experimentally determined constant—then we keep doubling it until it is not. We have thereby bracketed an admissible point. We then use bisection (we could just have easily used quadratic interpolation) to find an admissible point on this interval. The step size that we compute becomes the current step size, which we use as our first guess on the following iteration. This adaptive procedure does a good job of staying close to the optimal step size while performing a number of gradient computations that is proportional to the logarithm of the ratio between the previous step size and the current one.

8. Making the Gradient Time-Dependent

Thus far, we have treated the graph drawing problem as consisting of three somewhat independent subproblems: defining the force laws that quantify the aesthetic criteria, computing the forces so as to obtain the negative gradient of an implicit energy function, and performing numerical optimization to obtain a local minimum with respect to this energy function.

In this chapter, we consider strategies that make the gradient time-dependent—that is, where we change the force laws from iteration to iteration. We use this time-dependence in three ways. The first is to make the gradient smoother in the earlier iterations in order to improve performance and avoid poor local minima. The second is to incorporate constraints into our model by converting them into exterior penalties. The third is to introduce additional degrees of freedom so that the drawing space has more maneuvering room—e.g., turning a two-dimensional problem into a three-dimensional one—and then to treat the original problem as a constrained problem in the larger space.

8.1. Making the Gradient Smoother in the Early Iterations

The performance of a first-order optimization procedure, such as steepest descent or the conjugate gradient method, reflects the smoothness of the objective function. The less that the objective function looks like a linear or quadratic function, the longer it takes for an optimization procedure to converge. By making the force laws time-dependent, we can mitigate the effects of the non-smoothness of our energy function.

The spring forces, as long as we model them with a low-order polynomial, tend to be fairly well behaved. If we were to use a linear spring force law with a rest length of zero, then the spring energies (that is, their contributions to the objective function) would all be quadratic functions. Indeed, if we only had to contend with spring forces, we would require relatively few iterations for the optimization procedure. Unfortunately, it does not seem possible for us to do so without “densifying” the graph as Kamada and Kawai do in their model, associating a spring with every pair of vertices. Hence, we are stuck with the highly non-linear repulsion forces.

The vertex-vertex repulsion forces are poorly behaved both when the vertices are very near each other and when they are far away. When they are near each other, the

magnitude of the repulsion force abruptly approaches infinity. When they are far apart, the magnitude very slowly approaches zero. Both of these behaviors impede the optimization procedure, but we can address them by making the gradient time-dependent.

8.1.1. Capping Spikes

Assigning two vertices to identical coordinates drives the magnitude of their repulsion force to infinity. We, like Fruchterman and Reingold, handle the singularity arising from this situation by randomly moving the vertices a small distance away from each other.

This perturbation strategy, however, ignores a larger issue—namely, that the objective function behaves poorly in the neighborhood of the singularity. We refer to this region of poor behavior as a *spike*. In the vicinity of a spike, the term of the gradient associated with the spike dominates the overall gradient and thus causes the Hessian to be ill-conditioned. Regardless of how we choose our search direction, we will find that the step size becomes very small in the vicinity of a spike, since the optimization procedure must slowly maneuver around it. Both linear and quadratic models of the objective function are very inaccurate in the vicinity of a spike.

Spikes can also trap us in poor local minima. Because the objective function increases dramatically in the vicinity of a spike, the spike can create a local minimum that could easily be avoided if the optimization algorithm were able to jump over the spike.

Fruchterman and Reingold do not explicitly discuss the problems caused by spikes; nonetheless, their “cooling schedule” addresses them implicitly. Their algorithm limits the maximum vertex displacement per iteration as a linearly decreasing function of time, which they call the “temperature” of the drawing. The effect of their approach is similar to that of placing a time-dependent maximum on each vertex’s component of the gradient.

We take a slightly different approach. Rather than compute the gradient and then truncate each of its components, we truncate each repulsion term’s contribution to the gradient. We enforce a maximum magnitude on each vertex-vertex and vertex-edge repulsion force vector, without changing any of their directions, and make this maximum magnitude an increasing function of the number of iterations. By capping the magnitudes of the repulsion terms, we prevent spikes from interfering with the early iterations and possibly trapping us in poor local minima.

A simple way to cap the magnitudes is to make the maximum magnitude proportional to the number of iterations. This strategy is analogous to Fruchterman and Reingold's temperature scheme. Alternatively, we could start off with a small cap and increase it as the magnitude of the overall gradient decreases. Both strategies, like Fruchterman and Reingold's temperature scheme, require experimentation to tune the constants.

We still have to use perturbation to break symmetry if two vertices have identical coordinates or if a vertex and an edge are collinear, but at least we don't have to contend with an ill-conditioned Hessian.

8.1.2. Strengthening the Long-Range Vertex-Vertex Repulsion Forces

Now that we have dealt with spikes, we address the other problem caused by vertex-vertex repulsion forces: their slow convergence to zero as the vertices move far apart. Vertex-edge forces do not have this problem, because they are purely short-range.

In our discussion of the force model, we argued that the long-range vertex-vertex repulsion forces should be weak to avoid creating pockets of excessive local density in the drawing. Now, we are saying that weak long-range forces slow down the optimization process.

We reconcile these two issues by making the long-range forces stronger in the early iterations and weaker in the later ones. The early iterations will produce a drawing with the right shape, but perhaps with too much local density. The later iterations, by weakening the long-range repulsion forces, will spread out the pockets of local density.

As with the capping of spikes, we need to tune the weakening of long-range forces experimentally. We implement the weakening by using a convex combination of the strong and weak long-range repulsion laws. In other words, we make a linear combination, weighting the strong force by α and the weak force by $1 - \alpha$, where α is 1 on the first iteration and slowly decreases to 0 as a function of the number of iterations. Again, we determine the rate of decrease experimentally.

8.2. Using Exterior Penalties to Incorporate Constraints

Most of the force-directed algorithms treat graph drawing as an unconstrained optimization problem. At best, they allow the user to assign relative weights to the

different forces. Little work has addressed the problem of general graph drawing with constraints. A few approaches allow the user to fix the positions of particular vertices. The most relevant work, that of He and Mariott [HM96], allows only linear equalities and inequalities as constraints.

The possibility of specifying constraints makes a graph drawing algorithm more flexible. A user might introduce constraints to anchor certain vertices at fixed positions or to restrict them to particular regions of the drawing space. Constraints can also control the positions of vertices relative to one other, thus portraying clusters of vertices or particular relationships among the constrained vertices.

We incorporate constraints into our model by using the *method of exterior penalties*. This method requires, for each constraint, an efficient procedure to measure the distance (in \mathbf{R}^{2n}) from an infeasible drawing to the nearest drawing that satisfies the constraint. We use these procedures to add penalty terms to the objective function that increase over time, so that eventually all descent directions will point towards the feasible space.

Several caveats are in order.

First, the method of exterior penalties is not applicable to infeasible problems—that is, problems for which no solution satisfies all of the constraints. These problems are better addressed by a two-phase approach that first chooses a subset of constraints to be satisfied and then solves the resulting constrained optimization problem.

Second, the method can break down when the feasible space is disconnected. A one-dimensional example illustrates this possibility. Let us imagine that we have a single variable x , a trivial objective function that is always equal to 1, and two constraints. The first constraint is that $x \in [1, 2] \cup [3, 4]$; the second is that $x \in [-2, -1] \cup [3, 4]$. Let us imagine that we start with the infeasible point $x = 0$. The penalty term for the first constraint will point us in the positive direction, towards the nearest point that satisfies the constraint, $x = 1$. The penalty term for the second constraint, however, will point us towards $x = -1$. Because these two terms will cancel out, we will never find the feasible space, which is $x \in [3, 4]$.

Third, the magnitudes of the penalty terms should not be too large relative to the magnitude of the gradient. They should be just large enough to force the optimization

procedure towards the feasible space. If we make the penalties too large, then they will create the problems of spikes that we discussed earlier. Often, we do not have to make the penalties very large for the optimization procedure to discover the feasible space.

We have had good results with quadratic penalty terms. For each constraint, we make the corresponding penalty term the square of the vector difference between the current drawing and the closest drawing that satisfies the constraint. We call the negative gradient of the sum of all such penalties the *penalty vector*, and we add a multiple of this penalty vector to the negative gradient that we compute from the force laws.

Let us denote the penalty vector by \mathbf{p} and the negative gradient by $-\mathbf{g}$. Let θ be the angle between \mathbf{p} and $-\mathbf{g}$, i.e. $\cos \theta = \mathbf{p} \cdot (-\mathbf{g}) / \|\mathbf{p}\| \|\mathbf{g}\|$. Then, if $\cos \theta$ is positive, ignoring \mathbf{p} and following the negative gradient will bring us closer to the feasible space, while, if $\cos \theta$ is negative, doing so will take us away from the feasible space. The more negative the cosine, the greater we need to make our coefficient for \mathbf{p} .

In our implementation, this coefficient is $\max(\epsilon, \epsilon - \cos \theta) * \max(1, (\|\mathbf{g}\| / \|\mathbf{p}\|))$, where $\epsilon = 10^{-8}$. The first factor uses the cosine to weight the penalty vector, while the second factor normalizes the negative gradient and penalty vectors. This formula is surely not optimal, but it works well in practice and is simple to compute.

We refer the reader to Gill, Murray, and Wright [GMW81] for further discussion of the method of exterior penalties and related numerical optimization methods.

8.3. Introducing Additional Degrees of Freedom

Our last application of scheduling is to take an unconstrained graph drawing problem and turn it into a constrained problem in a larger drawing space, which we solve using exterior penalties. We transform the problem in order to take advantage of the maneuvering room in the larger space.

Before describing this technique, let us consider an example of what happens when the drawing space has only one dimension rather than two. We take a simple undirected graph: three vertices $\{\mathbf{v}_1, \mathbf{v}_2, \mathbf{v}_3\}$ and two edges $\{\mathbf{e}_1 = (\mathbf{v}_1, \mathbf{v}_2), \mathbf{e}_2 = (\mathbf{v}_2, \mathbf{v}_3)\}$.

The drawing on the left in Figure 8.1 shows the globally optimal drawing. Unfortunately, a local optimization procedure will only converge to this optimum (or its mirror image) if

v_2 is between v_1 and v_3 in the initial drawing. If the initial placement is random, this happy event occurs with probability $1/3$. With probability $2/3$, a local optimization procedure will converge to the drawing on the right (or one of the three other equivalent drawings), which is locally optimal but lousy.



Figure 8.1: Local optima for a 3-vertex graph in one dimension.
The drawing on the left is globally optimal.

While one-dimensional graph drawing may seem a contrived problem, it arises in code and data layout applications [Be94]. In any case, using local optimization methods in one dimension is clearly a poor strategy. A much better approach is to move the problem to a two-dimensional space and then somehow squash it back onto one dimension. In two dimensions, the graph above would, with probability 1, be drawn as some rotation of the global optimum.

How do we squash the problem back onto its original drawing space? In this example, we can introduce the constraint $y_i = 0$ for each vertex v_i . We then apply the method of exterior penalties to solve the constrained problem.

We can use this same strategy to convert an unconstrained two-dimensional problem into a constrained three-dimensional problem. Here, the constraint is $z_i = 0$ for each vertex v_i , and the corresponding penalty terms are z_i^2 . By lifting the problem from two dimensions to three or more dimensions, we can often “untwist” drawings that would otherwise converge to poor local minima.

9. Vertex Size and Shape

Thus far, we have used a force model in which vertices are represented by dimensionless points. While doing so has simplified our discussion thus far, we must take vertex size and shape into consideration in order to make our graph drawing algorithm relevant to practical problems.

In this chapter, we adapt the force laws to take into account vertex shape and size. We require that the vertex shapes are convex; if they are not, we can satisfy this requirement by replacing a vertex shape with its convex hull. We also require, for the sake of efficiency, access to a constant-time test that determines if and where a single line segment intersects the boundary of a given vertex. Such a test is straightforward when the vertices are drawn as rectangles, as is most commonly the case.

Vertex size and shape affect our force laws for edge springs, vertex-vertex repulsion, and vertex-edge repulsion. When vertices are large, we need to modify our force laws to make room for them. The modifications should be primarily short-range, since the size and shape of a vertex rapidly decrease in importance as we move away from it.

9.1. Vertex Radii

It is convenient to always measure the distance between two vertices by using the line segment connecting the vertex centers. We have to consider, however, that the distance between the vertex boundaries depends on the size and shape of the vertices, as well as the orientation of the line segment. In particular, we have to subtract out the “radius” of each vertex—that is, the distance from the center of each vertex to the point at which the line segment intersects the vertex boundary. We refer to these distances as the *radii* of the vertices with respect to the line segment connecting them. When there is no ambiguity, we simply refer to them as the vertex radii.

Figure 9.1 shows how we measure the radii of vertices v_1 and v_2 when we are computing the distance between them. We first draw the line segment connecting the vertex centers, and then we compute the distances between the centers and the intersections of this line segment with the vertex boundaries to obtain the vertex radii r_1 and r_2 .

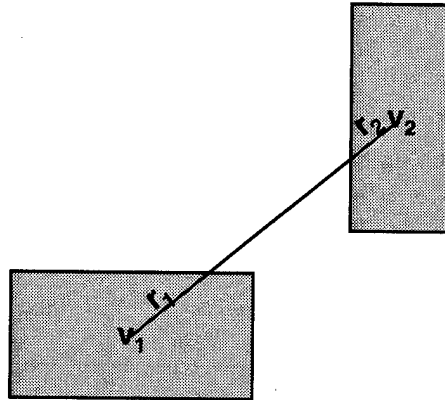


Figure 9.1: The radii of rectangular vertices v_1 and v_2 with respect to the line segment connecting them.

9.2. Adapting the Force Laws to Consider Vertex Radii

In order to take vertex radius into account, we make several changes to the force laws. First, we give the edge springs a non-zero rest length that reflects the radii of the endpoints with respect to the edge. Then, we modify the vertex-vertex repulsion law in order to make the boundary-to-boundary rest length of an edge equal to k . Finally, we make a similar modification to the vertex-edge repulsion force.

9.2.1. Increasing the Rest Length of Edge Springs

In the force model we have described thus far, the springs have a rest length of zero—that is, they always try to pull their endpoints closer together. While this works well for dimensionless vertices, it does not make as much sense when vertices have nontrivial size and shape.

In order to reflect vertex size and shape, we make the rest length of an edge spring equal to the sum of the endpoint radii. Accordingly, the spring pushes the endpoints away from each other when the endpoints overlap, since the distance between the centers is less than the sum of the radii. When the endpoints are mutually tangent, the spring exerts no force on them. Finally, if the endpoints are further apart than the sum of their radii, then the spring pulls them towards each other.

For an edge connecting dimensionless vertices v_i and v_j , our formula for the magnitude of the spring force was $\|f_{spring}(v_i, v_j)\| = \|x_i - x_j\|^2 / k$.

If the radii of \mathbf{v}_1 and \mathbf{v}_2 with respect to the line segment connecting them are r_1 and r_2 , then we make the magnitude $\|f_{spring}(\mathbf{v}_i, \mathbf{v}_j)\| = (\|\mathbf{x}_i - \mathbf{x}_j\| - (r_1 + r_2))^2 / (k + (r_1 + r_2))$.

The direction of the spring force (pulling the vertices towards or pushing them away from each other) depends on whether $\text{dist}(\mathbf{v}_i, \mathbf{v}_j)$ is greater than or less than $r_1 + r_2$. A reminder: we measure $\|\mathbf{x}_i - \mathbf{x}_j\|$ as the length of the line segment connecting the vertex centers.

9.2.2. Modifying the Vertex-Vertex Repulsion Law

We had set up our edge spring and vertex-vertex repulsion laws so that an edge would have a rest length of k . Now that we have modified the spring law to consider the vertex radii, we need to make a corresponding change to the vertex-vertex repulsion law.

For dimensionless vertices, we had the following formula for the magnitude of the repulsion force: $\|f_{repulsion}(\mathbf{v}_i, \mathbf{v}_j)\| = k^2 / \|\mathbf{x}_i - \mathbf{x}_j\|$.

If the radii of \mathbf{v}_1 and \mathbf{v}_2 with respect to the line segment connecting them are r_1 and r_2 , then we replace this formula with $\|f_{repulsion}(\mathbf{v}_i, \mathbf{v}_j)\| = (k + (r_1 + r_2))^2 / \|\mathbf{x}_i - \mathbf{x}_j\|$.

As we discussed earlier, using a single law for vertex-vertex repulsion can cause excessive local density. If we distinguish between strong short-range and long-range repulsion, then the above law is for short-range repulsion, and the modification to the inverse-square long-range repulsion law is analogous.

9.2.3. Modifying the Vertex-Vertex Repulsion Law

Finally, we need to modify the vertex-edge repulsion law to reflect the vertex size and shape.

In our model for dimensionless vertices, we made the magnitude of the vertex-edge repulsion force $\|f_{repulsion}(\mathbf{v}_i, \mathbf{e}_j)\| = c_{ve}((k^2 / x) - k)$ when x , the distance between vertex \mathbf{v}_i and edge \mathbf{e}_j , is less than k .

Applying the same idea we used for vertex-vertex repulsion, we replace k by $k + r$, where r is the radius of \mathbf{v}_i with respect to the shortest line segment connecting it to \mathbf{e}_j . Accordingly, the new magnitude is $\|f_{repulsion}(\mathbf{v}_i, \mathbf{e}_j)\| = c_{ve}(((k+r)^2 / x) - (k+r))$ when x , the distance between the center of vertex \mathbf{v}_i and edge \mathbf{e}_j , is less than $k + r$.

9.3. Adapting the Procedure to Compute the Forces

Since we are modifying the force laws to take vertex size and shape into account, we also have to make changes to the procedure for computing the forces. In particular, we have to modify the Barnes-Hut algorithm that we use for computing vertex-vertex repulsion and the distance cut-off procedure that we use for computing vertex-edge repulsion. We will assume for simplicity that all vertices are rectangles, but our methods apply as long as the vertices conform to simple, parameterized class of shapes, such as ellipses.

The change we make to the Barnes-Hut procedure is that we store in each cell the average shape of a vertex. Since our vertices are rectangles, we simply maintain the average width and height of the vertices in each cell. Then, when we approximate the repulsion that the cell exerts with its centroid, we use this width and height in our computation.

For our computation of vertex-edge repulsion, we have to modify the assignment of vertices to grid cells to take radius into account. We store each vertex in every grid cell that it intersects. Then, when we iterate for each edge through the grid cells it occupies (including all of the grid cells occupied by the endpoints) and the neighbors of those cells, we will find all vertices within the short range of the edge.

10. Qualitative Results: A Gallery of Examples

Until now, we have focused on the details of our algorithm. Now, we look at the performance of an implementation that we have written in Java. In this chapter, we take a qualitative perspective: we present a variety of drawing produced by our implementation and discuss the strengths and weakness of the algorithm on different classes of graphs in intuitive terms. In Chapter 11, we will take a more quantitative perspective.

Our presentation of drawings is in order of increasing density. We start from trees, the sparsest of graphs, and work our way up to complete graphs. We only consider graphs that are connected, since it is not difficult to find the connected components of a graph and draw them separately.

10.1. Trees

Trees are the sparsest of connected graphs: a tree of n vertices has $m = n - 1$ edges. Tree drawing is a well studied problem, and there are good, special-purpose algorithms for drawing both rooted (directed) and unrooted trees [RT81, Ea92].

It is surprising, perhaps, that force-directed algorithms perform very badly on trees. In fact, trees are some of the worst inputs for graph drawing algorithms based on numerical optimization. Trees have two qualities that confound force-directed algorithms. The first is that they have countless poor local minima that result from swapping the positions of subgraphs so that they cross. The second is that, because trees are so sparse, the spring forces do not particularly restrict the movement of vertices; instead, it is the repulsion forces that largely determine the placement of vertices. Because the repulsion forces are far less smooth than the spring forces, they slow down any first-order numerical optimization, such as steepest descent or the conjugate gradient method.

Nonetheless, we have two reasons to test our algorithm on trees. The first is completeness: since our algorithm applies to all connected graphs, it behooves us to test it on as wide a range of input graphs as possible. The other reason is that we can compare the performance of our algorithm with that of other force-directed approaches, and thereby see the relative strengths and weakness of our techniques.

The drawings that our algorithm produces are similar to those produced by radial tree drawing algorithms, only that ours tend to distribute vertices more evenly throughout the drawing area. Unlike the radial drawing algorithms, however, we do not always produce crossing-free drawings of trees. In general, drawings of trees that have edge crossings correspond to poor local minima.

We did experiment with modifying the force laws to produce more traditional drawings of rooted trees (see the discussion of “eumorphous” drawings in Section 3.1.1), where all edges were directed towards the root and pointed upwards. Unfortunately, we found that the aesthetic principles for eumorphous drawings of trees were very different from those for general graphs. While our force-directed drawings aim to distribute vertices uniformly throughout the drawing space, traditional drawings of rooted trees tend to be much denser at the bottom, where the leaves are, than at the top, where the root is, and they are generally much wider than they are tall.

Let us consider, for example, a complete binary tree of $n = 2^h - 1$ vertices. Our force-directed algorithm will produce a drawing that roughly occupies a square drawing area whose side is $k\sqrt{n}$. In contrast, a eumorphous drawing will have h layers and 2^{h-1} leaves—roughly half of the vertices—occupying the lowest of the layers. In order for the height and width of the drawing area to be equal, the vertical separation between layers would have to be $2^{h-1} / h$ (roughly $n / \log n$) times larger than the horizontal separation between vertices on the lowest layer.

We experimented with various schemes involving constraints and modifications of the spring laws for directed edges, but none of them consistently produced satisfactory drawings of rooted trees.

Given the difficulty that force-directed algorithms have drawing trees, we suspect that a general graph drawing algorithm should use a hybrid approach. First, it should compute the unique tree of biconnected components—that is, the maximal subgraphs that cannot be disconnected by the removal of a vertex. It should then use a specialized tree-drawing algorithm to arrange the centroids of these biconnected components. Finally, it should draw each component independently using a force-directed algorithm—with the centroids fixed according to the previous step. We discuss such an approach, as well as its pitfalls, in the section on future work.

We now present a few examples of trees produced by our algorithm.

Figure 10.1 shows a complete binary tree of 63 vertices. To produce this drawing, we used a three-dimensional drawing space with two-dimensional constraints, as described in section 8.3. Figure 10.2 shows an example of the many poor local minima that often result when we apply our algorithm directly on a two-dimensional drawing area.

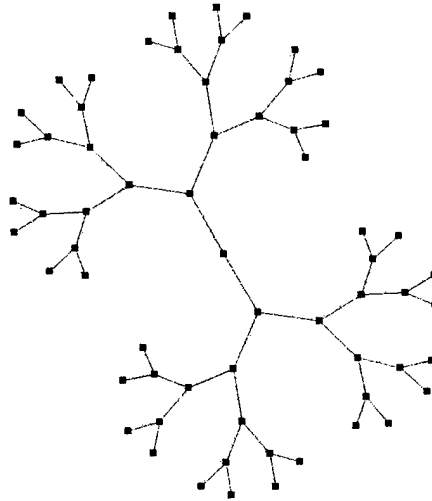


Figure 10.1: Complete Binary Tree of 63 Vertices

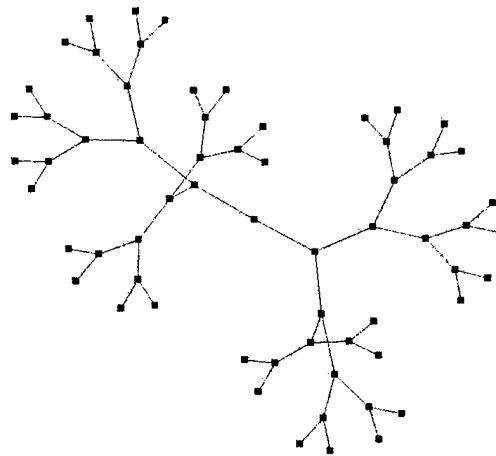


Figure 10.2: Example of Bad Local Minimum

Figure 10.3 shows a random tree of 100 vertices; here we can see clearly that the drawing is not radial, but rather that the vertices spread themselves out relatively uniformly throughout the drawing area.

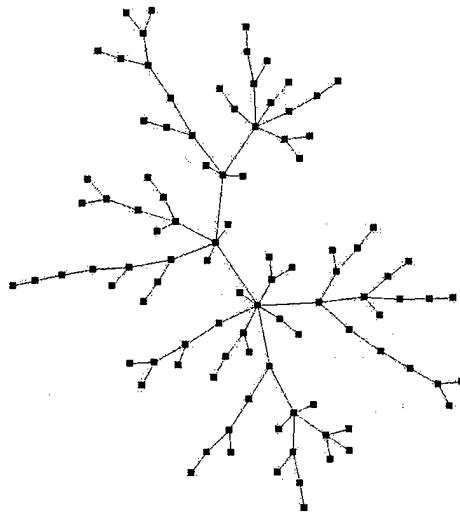


Figure 10.3: Random Tree of 100 Vertices

10.2. Planar Biconnected Graphs

As we have discussed, the performance of force-directed algorithms suffers for trees, and in general for graphs that are not biconnected. We therefore turn our attention to biconnected graphs. We start with an important class of biconnected graphs: graphs that are biconnected and planar.

Planar graphs are of particular theoretical and practical interest. Planar graphs, by definition, can be drawn in the plane without any edge crossings. Many classical results in graph theory pertain to planar graphs: Fary determined that a planar graph could be drawn without edge crossings using straight-line edges [Fa48]; Hopcroft and Tarjan determined how to both test the planarity of a graph and compute an embedding of it in linear time [HT74]; Tutte proposed a “barycenter” method for drawing planar graphs that was suggestive of the later force-directed approaches and that would always converge to a drawing without edge crossings [Tu60]. The practical significance of planar graphs comes from their ubiquity: maps are the face-duals of planar graphs; circuits laid out on a board cannot have edge crossings; roads and railroad tracks cannot arbitrarily cross each other; and so forth.

A classic result of Euler is that a planar graph of n vertices has at most $m \leq 3n - 6$ edges [BM76]. Planar graphs are therefore quite sparse: the average degree of a vertex is at most six.

In general, sparse graphs are harder for force-directed algorithms to draw than dense ones because the repulsion forces are not as smooth as the spring forces. Nonetheless, biconnected planar graphs are generally easier to draw than trees. The sparsest of biconnected planar graphs are cycles, where every vertex has a degree of two. Cycles, like trees, are susceptible to poor local minima because of their sparseness; these local minima generally result from the cycles getting tangled. At the other extreme, we have triangular meshes, where the average degree is almost six. These graphs, not surprisingly, are much easier for force-directed algorithms to draw.

Regardless of the planarity of the graph, our algorithm does not attempt to avoid edge crossings. Similarly, our algorithm does not treat graphs of three-dimensional objects in any special way—that is, the algorithm does not take into account the fact that their topologies correspond to those of three-dimensional objects.

Figure 10.4 shows a drawing of a cycle of 100 vertices. In general, cycles are optimally drawn as regular polygons. Interestingly, they are drawn as such even when placed in a higher dimensional space—that is, they will occupy a planar slice of that space.

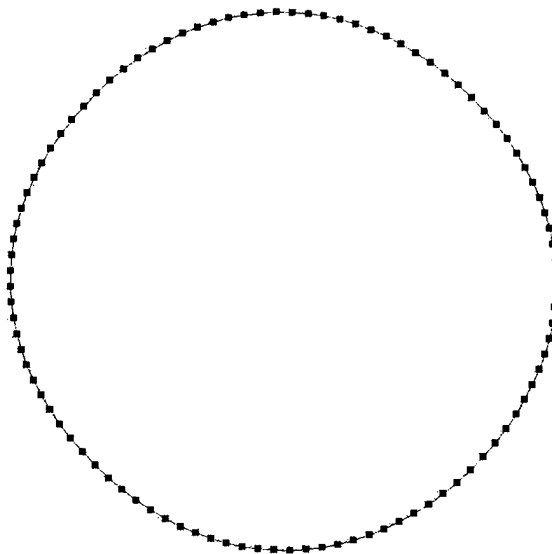


Figure 10.4: Cycle of 100 Vertices

Force-directed algorithms work especially well for planar meshes. Figure 10.5 shows a triangular mesh of 465 vertices. Figure 10.6 shows a square mesh of 400 vertices. As with trees, using a third dimension allows the drawing to untwist itself out of tangles. Like cycles, planar meshes will be drawn as planar even when placed in a higher dimensional space.

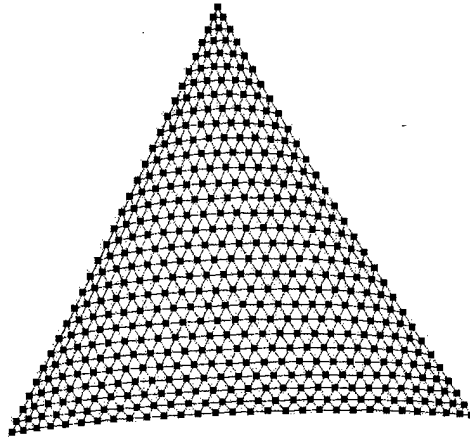


Figure 10.5: Triangular Mesh of 465 Vertices

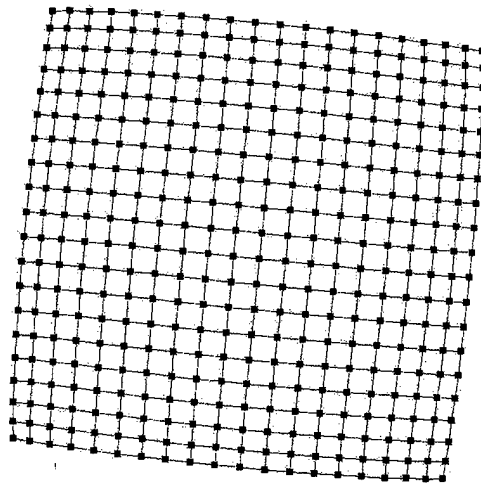


Figure 10.6: Square Mesh of 400 Vertices

Figure 10.7 shows two drawings of a graph corresponding to the topology of a dodecahedron. Interestingly, both graphs drawings were produced in two dimensions. Neither is crossing-free, since a crossing-free drawing would require a high variance in edge length. The drawing on the left appears to be three-dimensional.

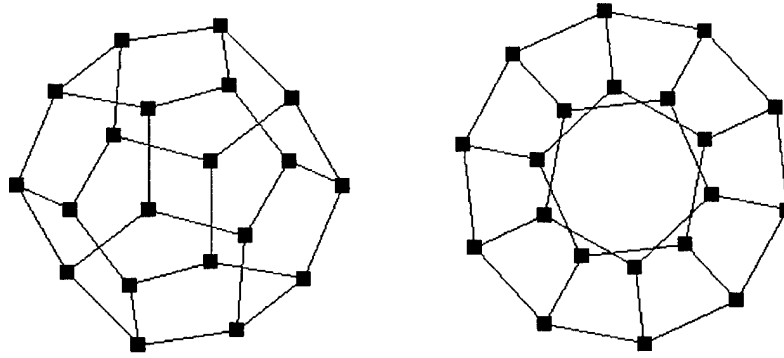


Figure 10.7: 2 Drawings of a Dodecahedron

Figure 10.8 shows a drawings of a triangular mesh of 210 vertices and a square mesh of 144 vertices constrained to occupy the surface of a three-dimensional sphere. This constraint is interesting for two reasons. First, it suggests applications such as cartography, where conforming the shape of the drawing surface is a critical part of the overall drawing problem. Second, the constraint is non-linear, and hence is not addressed by any of the published work on force-directed graph drawing.

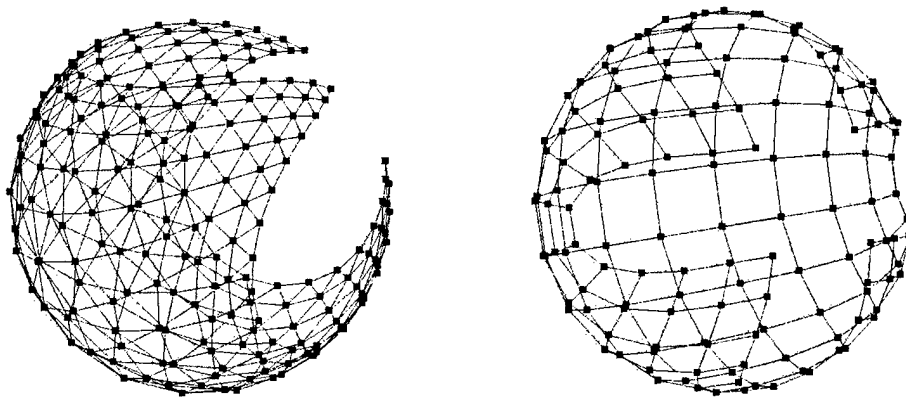


Figure 10.8: Planar Meshes Constrained to the Surface of a Sphere

10.3. Sparse Non-Planar Graphs

Although planarity arises naturally in graphs corresponding to concrete physical networks such as roads or railway systems, we can hardly expect abstract networks to be planar. Often, our graphs do not represent physical networks, but rather they represent relationships in an organization or interactions in a complex system. We may be able to assume that such graphs are sparse, but not that they are planar.

Our algorithm does not take edge crossings into account; rather, its performance depends mostly on the sparseness or density of the input graph. Of course, given a non-planar input graph, it will always produce a drawing that has edge crossings. In general, the denser the graph, the easier and faster it is for the numerical optimization procedure to converge to a local minimum. On the other hand, denser graphs often result in less legible drawings than sparser ones, because the edges clutter the drawing.

We have chosen examples for this section from two families of non-planar graphs where m is $\theta(n)$.

A cycle of n/c c -cliques (i.e. copies of K_c) is non-planar if $c \geq 5$ and has an average degree of roughly $c-1$. Figure 10.9 shows a cycle of 20 K_5 s.

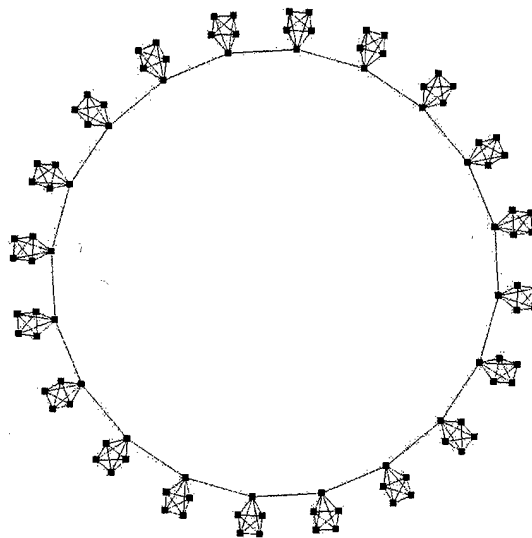


Figure 10.9: Cycle of 20 K_5 s

A torus is a non-planar graph constructed by taking a square mesh and connecting the top to the bottom and the left to the right. Every vertex in a torus has degree four. Figure 10.10 shows a torus of 256 drawn in both two and three dimensions. The drawing on the left misleadingly appears to be three-dimensional, but the drawing on the right, which is in fact three-dimensional, best reveals the structure of the graph.

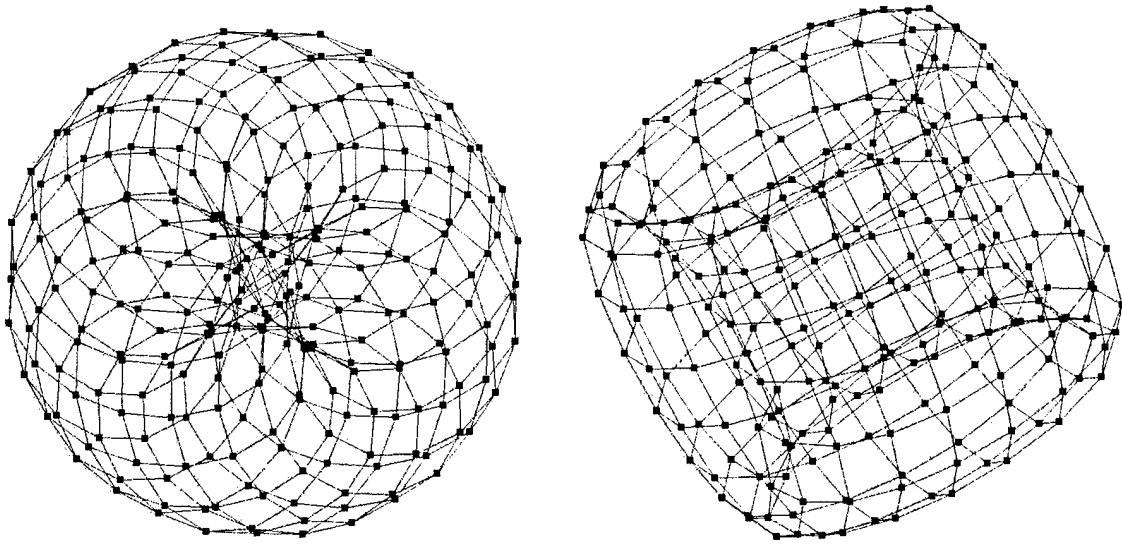


Figure 10.10: Torus of 256 Vertices in Two and Three Dimensions

10.4. Dense Graphs

Finally, we consider denser graphs where m is not $\theta(n)$. If m is $\theta(n \log n)$, then the time necessary to compute the spring forces will be within a constant factor of the time necessary to compute the vertex-vertex repulsion forces using the Barnes-Hut procedure. If m is $\theta(n^2)$, we have no reason to use the Barnes-Hut procedure: since we will require $\theta(n^2)$ time to compute the gradient, we may as well compute the repulsion forces exactly. In fact, we might even use Kamada and Kawai's algorithm, since we will already need $\theta(n^2)$ space to store the graph.

While increasing the density of a graph beyond an average degree of $\theta(\log n)$ increases the time necessary to compute the gradient, it does decrease the number of iterations necessary for convergence, since the spring forces are smoother than the repulsion forces, and the spring forces dominate the repulsion forces in dense graphs.

Most drawings of dense graphs are too cluttered with edges to be useful. Some exceptions are hypercubes, complete bipartite graphs, and complete graphs, like those we show below. We doubt that many practical applications require drawings of dense graphs, but we include this section for completeness.

A d -dimensional hypercube has 2^d vertices, each of degree d . Figure 10.11 shows drawings of a 6-dimensional hypercube of 64 vertices in drawing spaces of two and three dimensions.

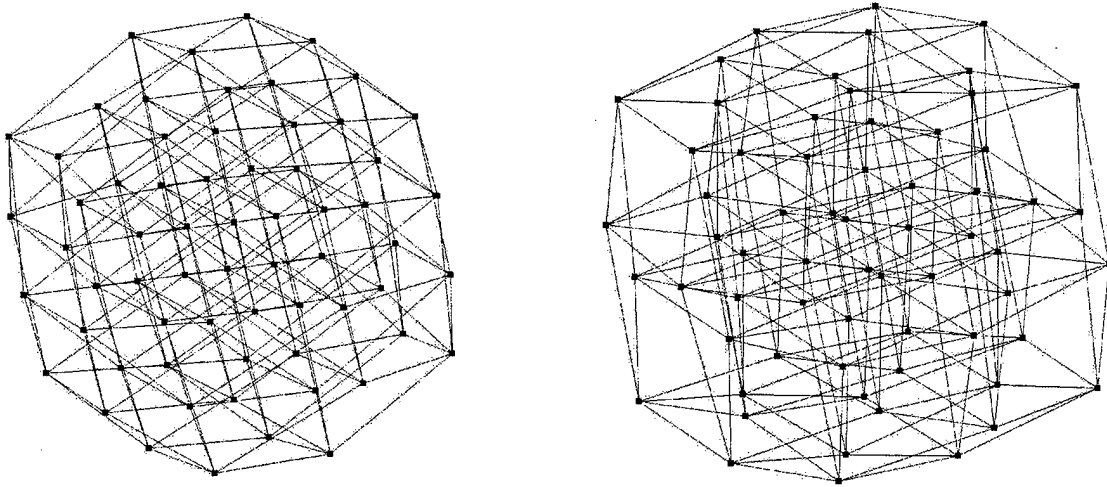


Figure 10.11: 6-Dimensional Hypercube in Two and Three Dimensions

The complete bipartite graph K_{n_1, n_2} has $n_1 + n_2$ vertices and $n_1 n_2 / 2$ edges. Figure 10.12 shows two two-dimensional drawings of $K_{6,6}$. In the drawing on the right, the vertices have been constrained to lie on a circle.

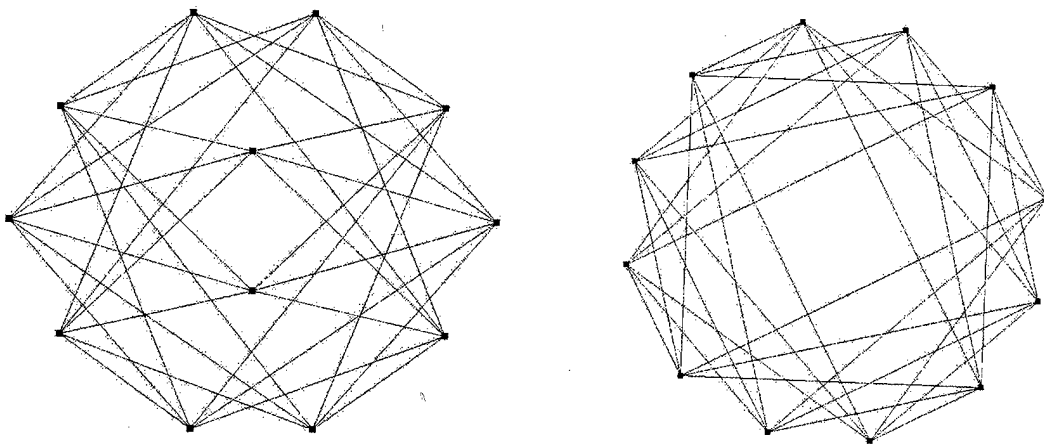


Figure 10.12: The Complete Bipartite Graph $K_{6,6}$

Finally, the complete graph K_n has n vertices, each of degree $n-1$. Figure 10.13 shows a two-dimensional drawing of K_{30} . We have made the vertices a bit larger so that they are clearer against the clutter of the 435 edges.

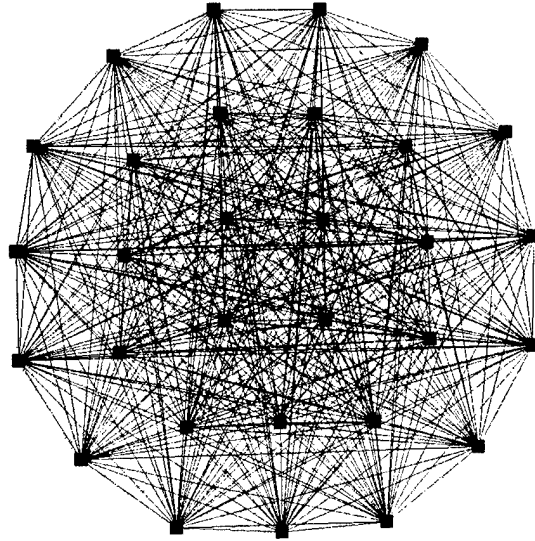


Figure 10.13: The Complete Graph K_{30}

11. Quantitative Results

While the previous chapter illustrates output generated by our algorithm, the drawings are fairly typical of those produced by all force-directed algorithms. Given that our main contribution is to improve the performance of such algorithms, we now shift to a more quantitative perspective to demonstrate this improvement.

We do so in three ways. First, we analyze our approach and compare it to others in terms of its computational complexity. Unfortunately, this analysis does not help us understand the number of iterations required to converge to a locally optimal drawing. We therefore perform experiments to see how the number of iterations required for convergence depends on both the size and density of the graph. Finally, we look at the time required to compute each of these drawings, and compare our times to those presented in other papers on force-directed algorithms.

We obtained all of our results with a Java implementation of our algorithm running on a Pentium 133 MHz machine under the Microsoft Windows 95 operating system. We used Sun Microsystems's JDK version 1.1.7 as our Java compiler and interpreter.

11.1. Computational Complexity

The computational complexity of an iteration, as shown in Chapter 6, is $\theta(m + n \log n)$. Briefly reviewing, we take $\theta(m)$ time to compute the spring forces, $\theta(n \log n)$ time to compute the vertex-vertex repulsion forces using the Barnes-Hut algorithm, and $\theta(m)$ time to compute the vertex-edge repulsion forces using distance cut-offs.

This computational complexity compares very favorably to those of other algorithms in the literature, as shown by the table in Figure 11.1. We note that, for the algorithms of Kamada and Kawai [KK89], Davidson and Harel [DH96], and Tunkelang [Tu94], we report the complexity of n iterations, since, for these three algorithms, each iteration only moves a single vertex as compared to moving all n vertices in all of the other algorithms. We also recall that Kamada and Kawai's algorithm uses a preprocessing phase that requires $\theta(n^2)$ space and $\theta(n^3)$ time. Finally, we note that some of the running times depend on the distribution of vertices being sufficiently uniform—namely, the computation of vertex-vertex repulsion forces in Fruchterman and Reingold's "grid variant" and computation of vertex-edge repulsion in our own algorithm.

	Springs	Vertex-Vertex Repulsion	Vertex-Edge Repulsion	Crossings	TOTAL
[Ea84]	$\theta(m)$	$\theta(n^2)$			$\theta(n^2)$
[FR91]	$\theta(m)$	$\theta(n^2)$ $\theta(n)$ for grid variant			$\theta(n^2)$ $\theta(m)$
[FLM94]	$\theta(m)$	$\theta(n^2)$			$\theta(n^2)$
[Tu94]	$\theta(m)$	$\theta(n^2)$ $\theta(n)$ for grid variant	$\theta(nm)$ $\theta(m)$	$\theta(m^2)$ $\theta(m)$	$\theta(m^2)$ $\theta(m)$
[KK89]	$\theta(n^2)$				$\theta(n^2)$
[DH96]	$\theta(m)$	$\theta(n^2)$	$\theta(nm)$	$\theta(m^2)$	$\theta(m^2)$
proposed algorithm	$\theta(m)$	$\theta(n \log n)$	$\theta(m)$		$\theta(m + n \log n)$

Figure 11.1: Computational Complexity of Computing the Negative Gradient

As we can see in the table, the computation of vertex-vertex repulsion forces is generally the bottleneck. The Barnes-Hut algorithm allows us to reduce the complexity of this step from $\theta(n^2)$ to $\theta(n \log n)$ without incurring the extreme loss of accuracy of the “grid variant” method (i.e. distance cut-offs). Unlike several of the algorithms, ours does take vertex-edge repulsion into account; unfortunately, including edge-crossings would not only be expensive, but would also rule out our optimization approach.

11.2. Number of Iterations

We have seen that the running time of our algorithm on a single iteration is asymptotically better than those of the published force-directed algorithms. We now look at the number of iterations required for convergence.

Unfortunately, all of the papers in the literature are evasive on this point. Most use a fixed number of iterations; Kamada and Kawai are the exception in that their termination condition depends on the maximum energy among the vertices. The authors that comment on the number of iterations generally speculate that it is proportional to the number of vertices. Unfortunately, there is no systematic study of the performance of graph drawing algorithms on large graphs, perhaps because the $\theta(n^2)$ inner loop of the published algorithms makes such a study prohibitive.

In order to gain some insight into the number of iterations required for convergence, we ran a suite of experiments. We used several families of graphs: paths, cycles, complete binary trees, square meshes, hypercubes, and complete graphs. For each family, we selected a set of graphs of varying sizes, in order to measure the number of iterations as a function of the size. In order to test the relative performance of steepest descent and the conjugate gradient method, we tested all of our graphs with both optimization procedures. For each graph and optimization procedure, we ran our algorithm ten times on random initial drawings, and then computed the mean number of iterations required for convergence. We used a straightforward, if conservative, convergence criterion: the algorithm terminates when an iteration moves no vertex more than half of a pixel. Since our line search is reasonably accurate, this criterion all but guarantees that the final drawing is visually indistinguishable from a local optimum.

The plots that follow confirm two observations that we have made in earlier chapters. First, the conjugate gradient method consistently outperforms steepest descent, and the gap widens as n increases. Second, the number of iterations required for convergence decreases as the density increases. We note that a conjugate gradient iteration is only slightly more expensive than that for a steepest descent iteration; in particular, computing the descent direction requires only one gradient computation in either case.

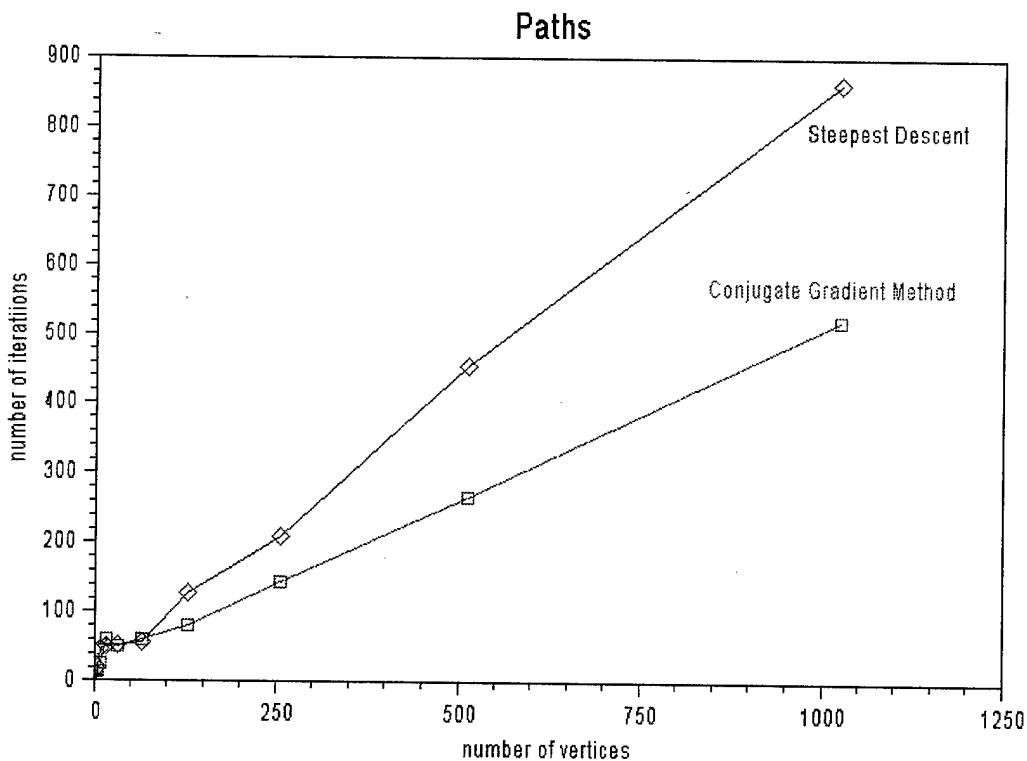


Figure 11.2: Performance on Paths

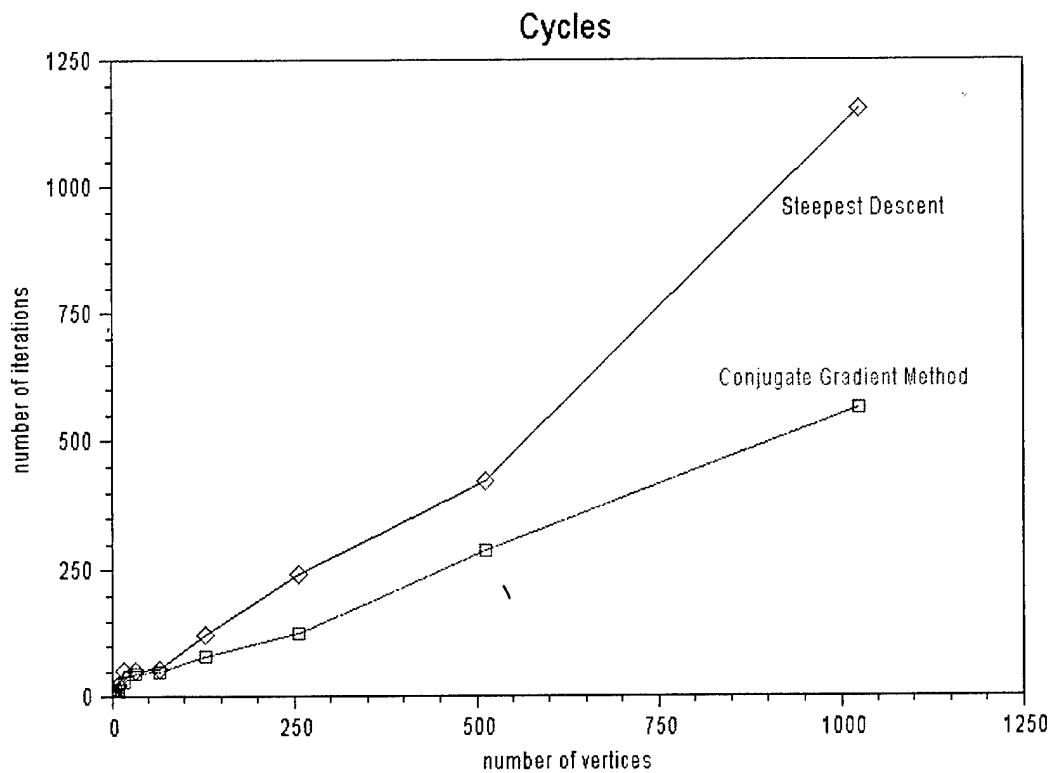


Figure 11.3: Performance on Cycles

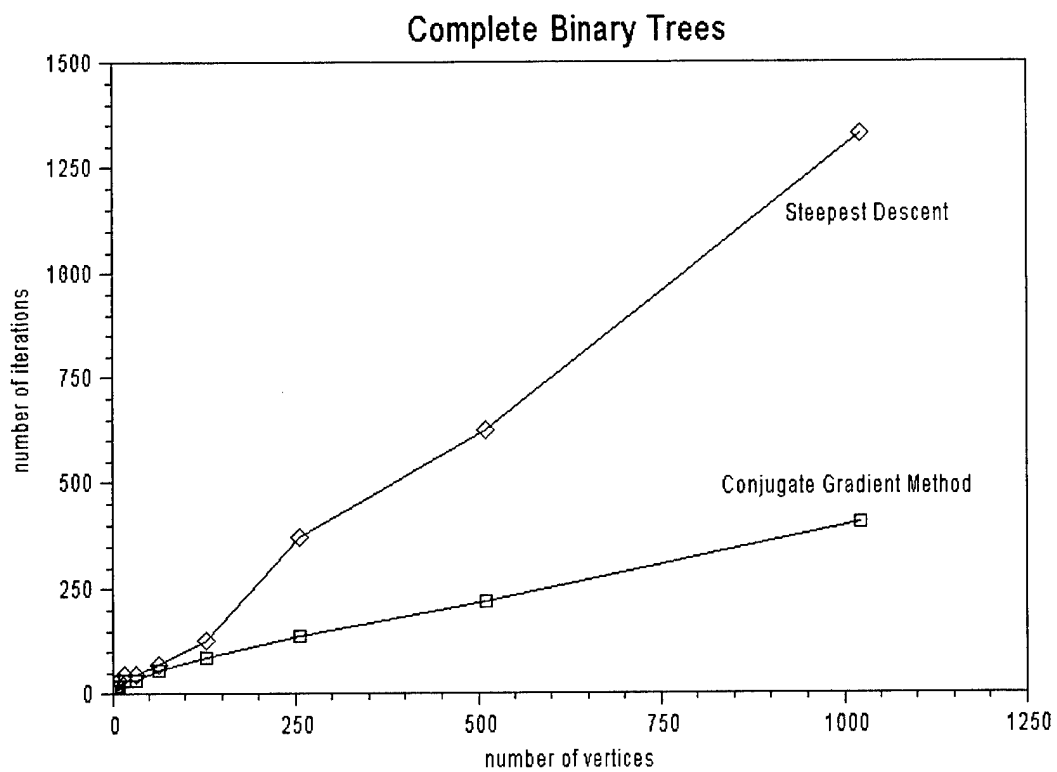


Figure 11.4: Performance on Complete Binary Trees

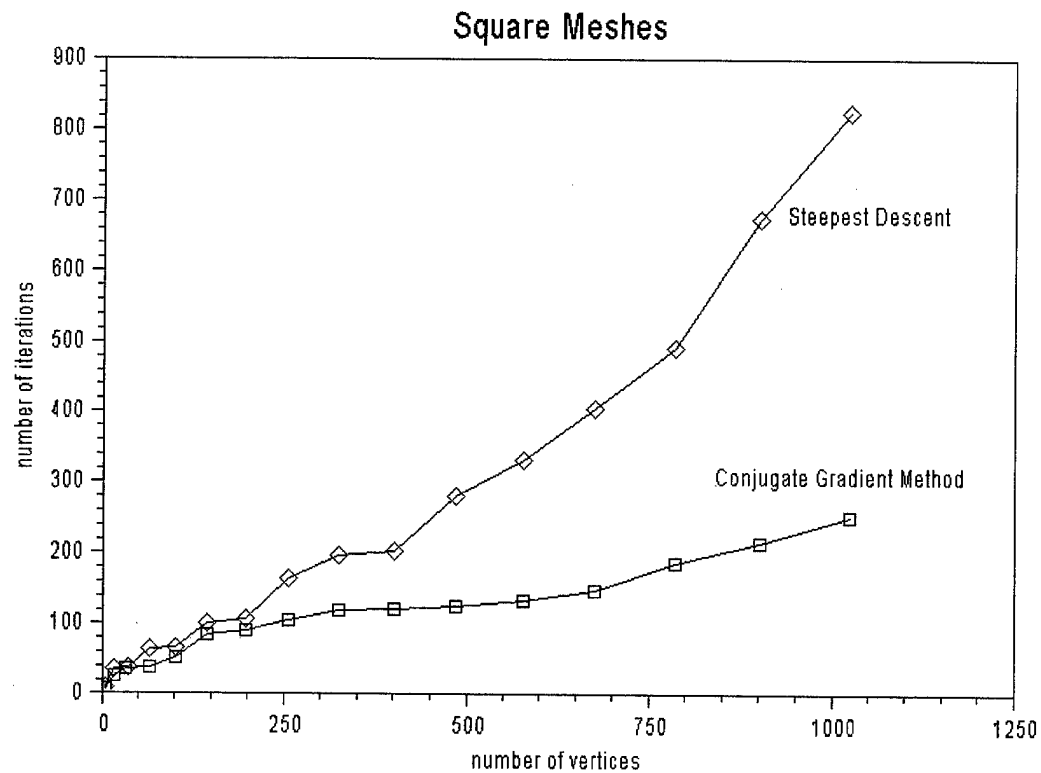


Figure 11.5: Performance on Square Meshes

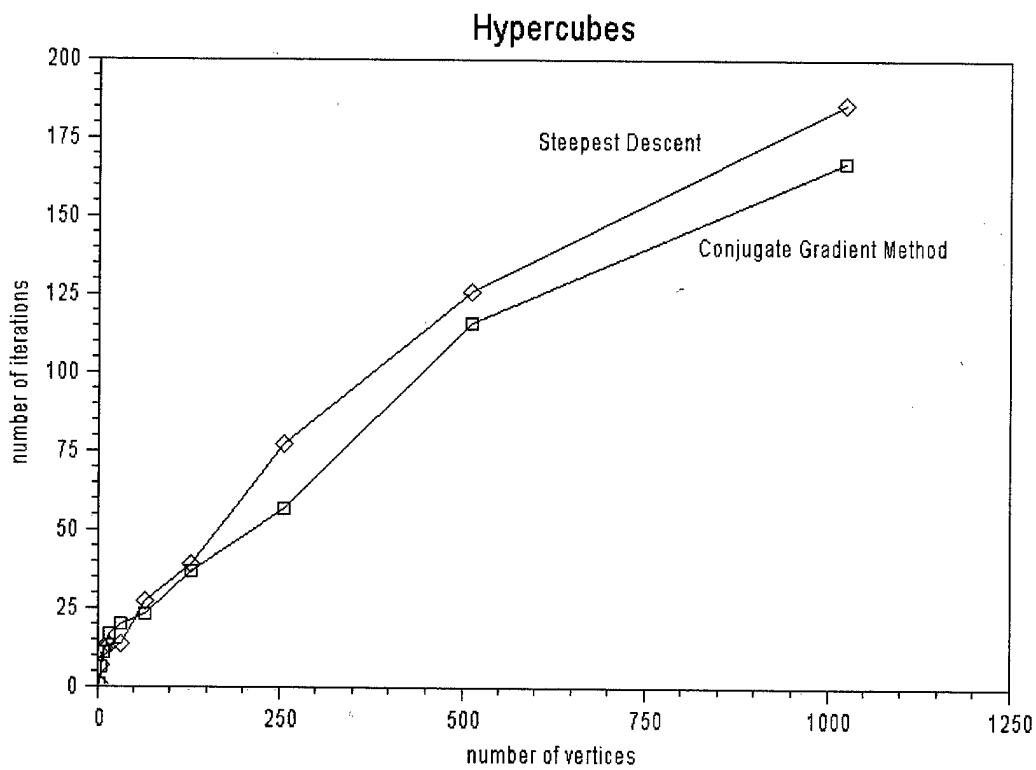


Figure 11.6: Performance on Hypercubes

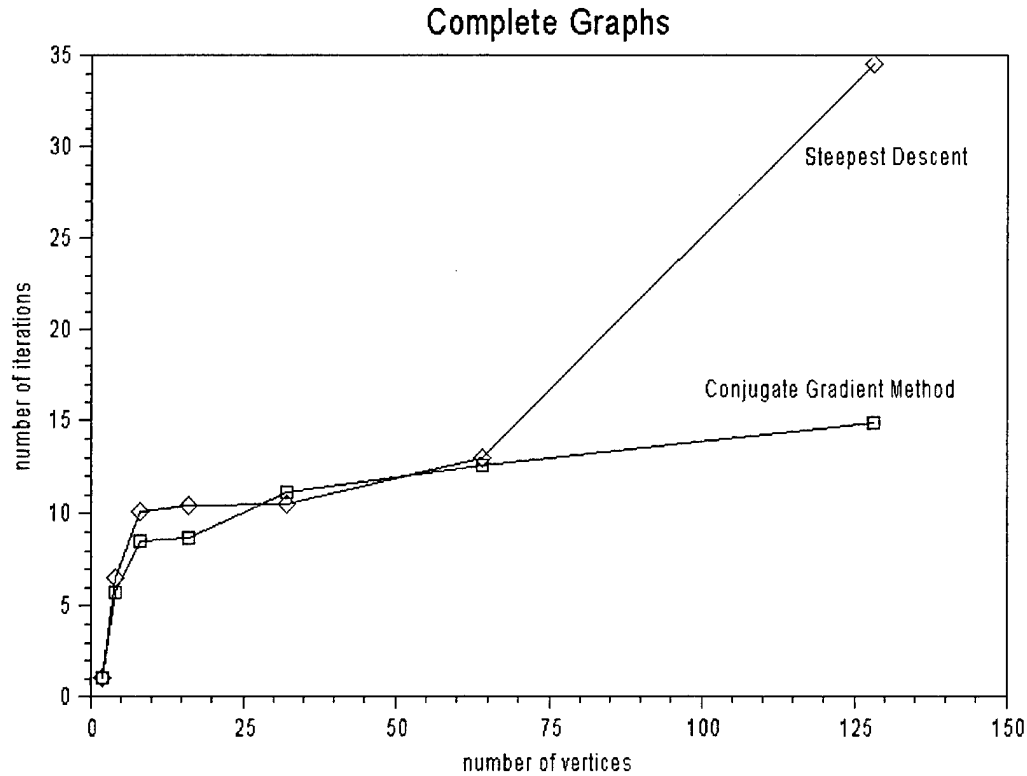


Figure 11.7: Performance on Complete Graphs

11.3. Running Time

A review of the literature reveals that very few papers even consider the performance of force-directed algorithms on large graphs. In fact, we could only find one paper that reported running times for graphs of over a hundred vertices.

Frick et al., report running times of 9.19 seconds for a complete binary tree of 127 vertices, 9.54 seconds for a path of 128 vertices, 45.04 seconds for a binary tree of 255 vertices, 37.93 seconds for a path of 256 vertices, and 71.78 seconds for a square mesh of 256 vertices. They estimate that the number of iterations is linear in the number of vertices, and hence that their running time is $\theta(n^3)$, which would imply that doubling the number of vertices would multiply the running time by eight.

Not only do we achieve better running times, but our algorithm scales more gracefully because of both the Barnes-Hut and conjugate gradient procedures. If we make the same assumption as Frick et al. that the number of iterations is linear in the number of vertices, then our running time is $\theta(n^2 \log n)$, which would imply that doubling the number of vertices roughly multiplies the running time by four. If, as convergence analysis of the

conjugate gradient method suggests, the number of iterations is proportional to the square root of the number of vertices, then this difference is even larger.

The plot below shows the running times for the families of graphs we have described in the previous section. As we can see, for graphs of the same number of vertices, the running time decreases as the density increases. Unfortunately, our implementation could not handle large complete graphs.

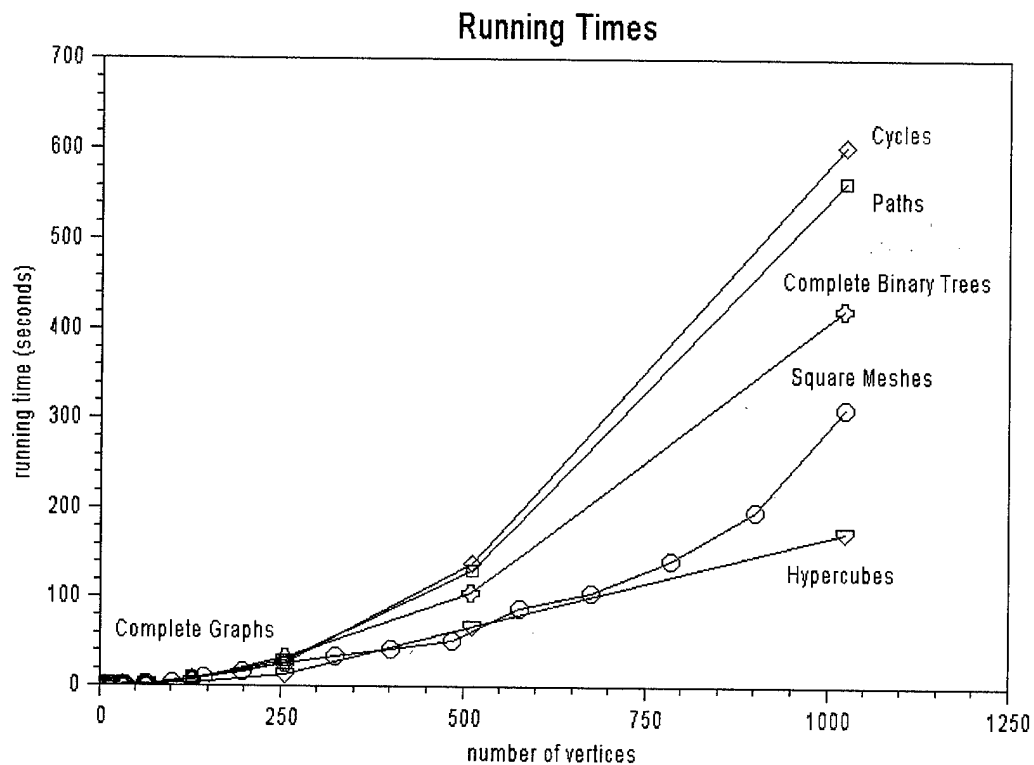


Figure 11.8: Running Times on a Variety of Input Graphs

12. Conclusions and Future Work

The principle contribution of this dissertation is to approach graph drawing using time-tested techniques from other fields. The original impetus for this work was an insight about replacing the fixed step size in published force-directed algorithms with a primitive line search procedure. Indeed, the adaptive line search procedure that we use is a major improvement on either using a fixed step size or complicating the algorithm with a “temperature” scheme. In general terms, however, we furthered the state of the art by not treating graph drawing as an isolated field.

From numerical optimization, we learned that we could achieve a better rate of convergence with conjugate gradients than with steepest descent. We also learned to pay better attention to the smoothness of the objective function. Finally, we were able to take advantage of the method of exterior penalties, both to incorporate a general class of constraints into our model and to avoid poor local minima.

From the many-body simulation literature, we borrowed the Barnes-Hut algorithm. This improvement is perhaps the most critical to making graph drawing scale to large graphs.

Finally, we had some new insights specific to graph drawing. In particular, our handling of vertex shape and size and our introducing a vertex-edge repulsion force make the general graph drawing model much more relevant to real visualization problems.

Of course, there are many open problems in graph drawing. Here are some questions that suggest directions for future work:

1) Can we make a rigorous theoretical analysis of the number of iterations required for convergence?

Both the method of steepest descent and the conjugate gradient method lend themselves to theoretical analysis. Indeed, the former can be shown to have a linear rate of convergence, while the latter can be shown to have a superlinear rate. A more accurate analysis of the rate of convergence requires that we know the condition number of the Hessian of the objective function we are minimizing. Since our objective function is not quadratic, the Hessian is not a constant, and therefore the condition number changes from

iteration to iteration. A deeper understanding of the convergence properties of different optimization procedures on graph drawing problems probably requires analytical techniques that specifically address this varying condition number.

2) Can we incorporate discrete terms, such as edge crossings, into a model based on continuous optimization?

There is a consensus in the graph drawing community that, all else equal, it is best to avoid edge crossings. Unfortunately, all else is not equal. The main problem with incorporating edge crossings into a continuous optimization approach is that the number of edge crossings is a discrete term. What would be ideal is a continuous term that correlates, at least approximately, to the number of edge crossings.

3) Can we design an algorithm that recognizes easy patterns in a graph and uses a divide-and-conquer approach to draw the graph more efficiently?

A first step in this direction would be to split a graph into its biconnected components, as we discussed in Section 10.1. To review, the idea is to lay out the centroids of the biconnected components using a specialized tree-drawing algorithm, and then to apply our force-directed algorithm to each biconnected component separately, fixing its centroid to where the tree-drawing algorithm placed it.

This approach, however, needs to address the subtlety that the edges connecting vertices in different biconnected components will be affected by the placement of their endpoints within their respective components. Moreover, it only helps us when we have a significant number of biconnected components. It would be nice to explore more sophisticated heuristics, such as partitioning the graph using small separators.

4) Can we do better than local optimization, e.g. can we obtain a drawing whose energy is within some constant multiple of the globally optimal energy?

This problem, as far as we know, has been completely open since Eades wrote his first paper on the spring model. An approach with guaranteed bounds in terms of the globally optimal energy would seem to require a much deeper understanding of the problem than we have thus far. We have nothing to offer but encouragement.

5) Can we achieve drawings that conform to the aesthetics of the force-directed model without resorting to continuous optimization?

The only techniques in the graph drawing literature that address general graphs are the topology-shape-metrics model and the force-directed model. The former only applies to orthogonal graph drawing problems. The latter, while useful, is fraught with problems, ranging from vulnerability to poor local minima to performance issues. Is there an alternative technique for producing drawings with the aesthetics that the force-directed model aims to quantify?

Bibliography

- [Be94] B. Beckman, "Theory of Spectral Graph Layout," Technical Report MSR-TR-94-04, Microsoft Research, 1994.
- [BH86] J. Barnes and P. Hut, "A Hierarchical $O(N \log N)$ Force-Calculation Algorithm," *Nature*, vol. 324, pp. 446-449, 1986.
- [BK94] T. Biedl and G. Kant, "A Better Heuristic for Orthogonal Graph Drawings," in *Proceedings of the Second Annual European Symposium on Algorithms*, vol. 855 of *Lecture Notes in Computer Science*, pp. 24-35, 1994.
- [BM76] J. Bondy and U. Murty, *Graph Theory with Applications*, Macmillan, London, 1976.
- [Ca80] M. Carpano, "Automatic Display of Hierarchized Graphs for Computer-Aided Decision Analysis," *IEEE Transactions on Systems, Man, and Cybernetics*, vol. 10, no. 11, pp. 705-715, 1980.
- [CLR90] T. Cormen, C. Leiserson, and R. Rivest, *Introduction to Algorithms*, MIT Press, London, 1990.
- [CP96] M. Coleman and D. Parker, "Aesthetics-based Graph Layout for Human Consumption," *Software—Practice and Experience*, vol. 26, no. 12, pp. 1415-1438, 1996.
- [DETT94] G. Di Battista, P. Eades, R. Tamassia, and I. Tollis, "Algorithms for Drawing Graphs: An Annotated Bibliography," *Computational Geometry*, vol. 4, pp. 235-282, 1994.
- [DETT99] G. Di Battista, P. Eades, R. Tamassia, and I. Tollis, *Graph Drawing*, Prentice-Hall, New Jersey, 1999.
- [DH96] R. Davidson and D. Harel, "Drawing Graphs Nicely Using Simulated Annealing," *ACM Transactions on Graphics*, vol. 15, no. 4, pp. 301-331, 1996.

- [Ea84] P. Eades, "A Heuristic for Graph Drawing," *Congressus Numerantium*, vol. 42, pp. 149-160, 1984.
- [Ea92] P. Eades, "Drawing Free Trees," *Bulletin of the Institute for Combinatorics and its Applications*, vol. 5, pp. 10-36, 1992
- [ES90] P. Eades and K. Sugiyama, "How to Draw a Directed Graph," *Journal of Information Processing*, vol. 13, no. 4, pp. 424-437, 1990.
- [Fa48] I. Fary, "On Straight Lines Representations of Planar Graphs," *Acta Scientiarum Mathematicarum*, vol. 11, pp. 229-233, 1948.
- [FCW67] C. Fisk, D. Caskey, and L. West, "ACCEL: Automated Circuit Card Etching Layout," in *Proceedings of the IEEE*, vol. 55, no. 11, pp. 1971-1982, 1967.
- [FLM94] A. Frick, A. Ludwig, and H. Mehldau, "A Fast Adaptive Layout Algorithm for Undirected Graphs," in [GD94], pp. 388-403.
- [FR91] T. Fruchterman and E. Reingold, "Graph Drawing by Force-Directed Placement," *Software—Practice and Experience*, vol. 21, no. 11, pp. 1129-1164, 1991.
- [GD93] G. Di Battista, H. de Fraysseix, P. Eades, P. Rosenstiehl, and R. Tamassia, eds., *Proceedings of ALCOM International Workshop on Graph Drawing and Topological Graph Algorithms (Graph Drawing '93)*, Paris, France, 1993.
- [GD94] R. Tamassia and I. G. Tollis, eds., *Proceedings of DIMACS International Workshop, GD '94*, Princeton, New Jersey, USA, vol. 894 of *Lecture Notes in Computer Science*, 1994.
- [GD95] F. J. Brandenburg, ed., *Proceedings of Symposium on Graph Drawing, GD '95*, Passau, Germany, vol. 1027 of *Lecture Notes in Computer Science*, 1995.
- [GD96] S. North, ed., *Proceedings of Symposium on Graph Drawing, GD '96*, Berkeley, California, USA, vol. 1190 of *Lecture Notes in Computer Science*, 1996.
- [GD97] G. Di Battista, *Proceedings of 5th International Symposium, GD '97*, Rome, Italy, *Algorithms*, vol. 1353 of *Lecture Notes in Computer Science*, 1997.

- [GJ83] M. Garey and D. Johnson, "Crossing Number is NP-Complete," *SIAM Journal of Algebraic and Discrete Methods*, vol. 4, no. 3, pp. 312-316, 1983.
- [GMW81] P. Gill, W. Murray, and M. Wright, *Practical Optimization*, Academic Press, London, 1981.
- [GNV88] E. Gansner, S. North, and K. Vo, "DAG—A Program that Draws Directed Graphs," *Software Practice and Experience*, vol. 18, no. 11, pp. 1047-1062, 1988.
- [GR87] L. Greengard and V. Rokhlin, "A Fast Algorithm for Particle Simulations," *Journal of Computational Physics*, vol. 73, pp. 325-248, 1987.
- [GT94] A. Garg and R. Tamassia, "On the Computational Complexity of Upward and Rectilinear Planarity Testing," in [GD94], pp. 12-23.
- [HM96] W. He and K. Mariott, "Constrained Graph Layout," in [GD96], pp. 217-232.
- [HT74] J. Hopcroft and R. Tarjan, "Efficient Planarity Testing," *Journal of the ACM*, vol. 21, no. 4, pp. 549-568, 1974.
- [Ig95] J. Ignatowicz, "Drawing Force-Directed Graphs using Optigraph," in [GD95], pp. 333-336.
- [KK89] T. Kamada and S. Kawai, "An Algorithm for Drawing General Undirected Graphs," *Information Processing Letters*, vol. 31, pp. 7-15, 1989.
- [PT98] A. Papakostas and I. Tollis, "Algorithms for Area-Efficient Orthogonal Drawings," *Computational Geometry: Theory and Applications*, vol. 9, nos. 1-2, pp. 83-110, 1998.
- [QB79] N. Quinn, Jr. and M. Breuer, "A Force Directed Component Placement Procedure for Printed Circuit Boards," *IEEE Transactions on Circuits and Systems*, vol. 26, no. 6, pp. 377-388, 1979.
- [RM88] M. Reggiani and F. Marchetti, "A Proposed Method for Representing Hierarchies," *IEEE Transactions on Systems, Man, and Cybernetics*, vol. 18, no. 1, pp. 2-8, 1988.

- [RT81] E. Reingold and J. Tilford, "Tidier Drawing of Trees," *IEEE Transactions on Software Engineering*, vol. 7, no. 2, pp. 223-228, 1981.
- [Sa90] J. Salmon, *Parallel Hierarchical N-Body Methods*, PhD Thesis, California Institute of Technology, 1990.
- [SM94] K. Sugiyama and K. Misue, "A Simple and Unified Method for Drawing Graphs: Magnetic-Spring Algorithm," in [GD94], pp. 364-375.
- [SR83] K. Supowit and E. Reingold, "The Complexity of Drawing Trees Nicely," *Acta Informatica*, vol. 18, pp. 359-368, 1983.
- [STT81] K. Sugiyama, S. Tagawa, and M. Toda, "Methods for Visual Understanding of Hierarchical System Structures," *IEEE Transactions on Systems, Man, and Cybernetics*, vol. 11, no. 2, 1981.
- [SW94] J. Salmon and M. Warren, "Skeletons from the Treecode Closet," *Journal of Computational Physics*, vol. 111, no. 1, 1994.
- [Ta87] R. Tamassia, "On Embedding a Grid with the Minimum Number of Bends," *SIAM Journal of Computation*, vol. 16, no. 3, pp. 421-444, 1987.
- [Tu60] W. Tutte, "Convex Representations of Graphs," in *Proceedings of the London Mathematical Society*, vol. 10, no. 3, pp. 304-320, 1960.
- [Tu63] W. Tutte, "How to Draw a Graph," in *Proceedings of the London Mathematical Society*, vol. 13, no. 3, pp. 743-768, 1963.
- [Tu94] D. Tunkelang, "A Practical Approach to Drawing Undirected Graphs," Technical Report CS-94-161, Carnegie Mellon University School of Computer Science, 1994. Presented at [GD93].
- [WM95] X. Wang and I. Miyamoto, "Generating Customized Layouts," in [GD95], pp. 504-515.
- [WS79] C. Wetherell and A. Shannon, "Tidy Drawing of Trees," *IEEE Transactions on Software Engineering*, vol. 5, no. 5, pp. 514-520, 1979.